2.2 SITE FACTORS

2.2.1 RFD Gain/Loss

In the original site configuration, a small gain in each primary multicoupler provided sufficient margin to overcome cable losses in the RF Distribution System (RFD). Subsequent modifications to the RFD increased signal loss with the addition of higher loss cables, longer cable runs, and components with signal loss. In order to understand the full significance of these changes, the gains and losses of selected signal paths of the RFD were measured. The team determined the gain/loss values from the input of the primary multicouplers to a test output port of ENLARGER located in the RF Room. This measurement assumes that the cables from the antenna elements to the input of the primary multicouplers are in good condition; since these cables are frequently checked by the AN/FRM-19 system, this is considered a reasonable assumption. It also assumes that the additional loss in cables from the ENLARGER output ports to operating receiver systems is low.

The gains and losses were measured for the RF paths for Beams 084, 156, and 252. Table 2.2.1-1 provides the total signal loss of each path except for the beamformers. Loss values at and below the first 8-MHz values are for the low-band paths. Loss at and above the second 8-MHz values are for the high-band paths. Beamformer loss was determined by a separate measurement to be about 1 dB. This value must be added to the total loss values provided in Table 2.2.1-1.

The RFD loss values provided in this report represent those for normally functioning beams. Several beams were found to have faulty multicouplers, and the RFD loss for these beams was very high. Since site personnel were repairing the faulty multicouplers, their impact on signal reception is not considered in this document.

A plot of the signal loss values for the three beams examined is shown in Figure 2.2.1-1. The plot shows that the measured results are consistent from beam to beam. The relatively high value of low-band loss at 8 MHz was traced to the ENLARGER diplexer. The high-band loss at 8 MHz was also somewhat larger than expected. These two values suggest that the diplexer is not properly functioning at the low-band to high-band transition frequency. While the RFD loss at other frequencies is considered normal for an ENLARGER-equipped site, it indicates the capability to receive a significant number of low-level signals of interest (SOI) will be lost.

Table 2.2.1-1

RFD Signal Loss

Frequency MHz	Beam 084 dB Loss	Beam 156 dB Loss	Beam 252 dB Loss
2	7.3	7.5	7.9
4	6.3	7.5	7.8
6	7.1	7.8	8
8	15.3	14.1	14.4
8	8.3	7.1	7.4
10	5.1	5.1	4.9
12	5.2	4.9	5
14	6.2	5.2	5.4
16	6	5.4	5.7
18	6.4	5.8	6.1
20	6.7	5.9	6.4
22	6.8	6.4	6.5
24	6.7	6.2	6.5
26	6.7	6.1	6.5
28	6.8	6.5	6.4
30	6.2	5.9	6.5

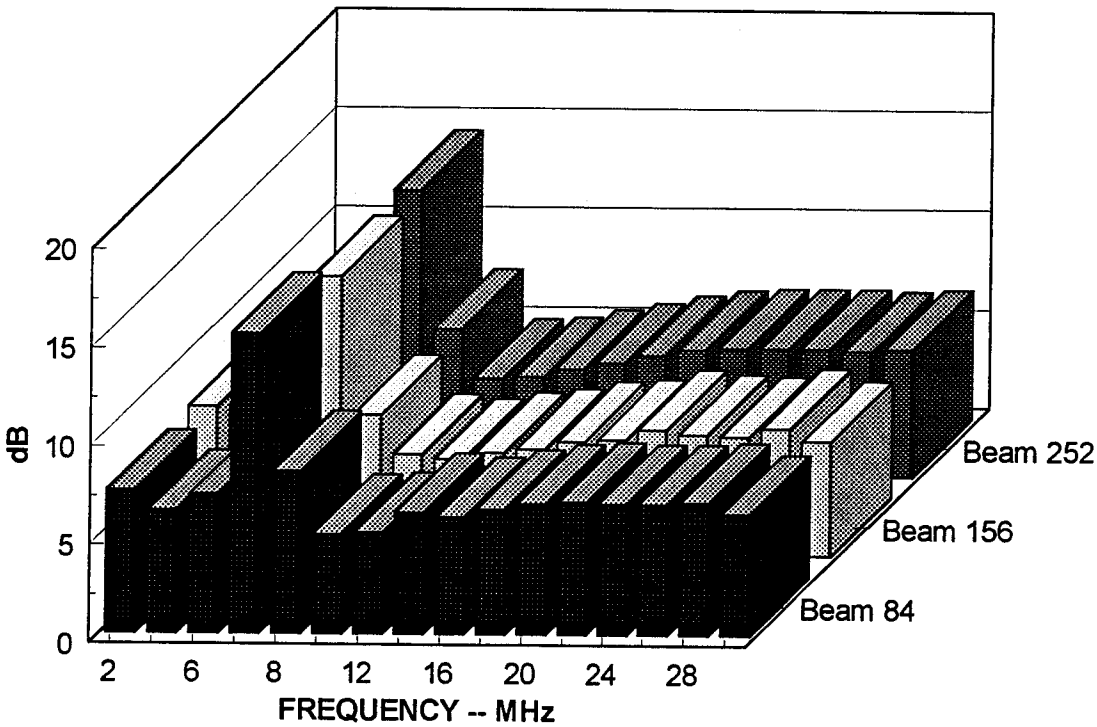

Figure 2.2.1-1

Plot of RFD Loss for Selected Beams

2.2.2 RFD Noise Floor

Three different kinds of RFD noise floor must be examined. The first kind is the noise floor of the primary multicouplers. This establishes the minimum detectable signal level for the site. Next, the noise floor of selected beams at the input terminals at a test receiver must be established. This requires that the inputs to the low- and high-band primary multicouplers forming each selected beam be terminated. This measurement establishes the additional noise added by components of the RFD. Also, it measures the amount of signal and noise that leaks into each test beam. Finally, the operating noise floor fed to a receiver during normal operation determines the present ability of a site's receiving system to detect a signal. The operating noise floor consists of site noise plus man-made noise and interference from both internal and external sources.

All final noise floor values are expressed in terms of the average noise level found in a 3-kHz gaussian-shaped bandwidth. This is the noise level shown by a spectrum analyzer with a gaussian-shaped bandwidth and with its bandwidth control set to 3 kHz. The noise floor of a standard receiver with a rectangular-shaped bandwidth will be somewhat lower than these values. The noise floor at wider bandwidths will also be higher and at narrower bandwidths will be lower than the measured values. The 3-kHz value is used since it represents the bandwidth of several typical receiving systems.

The noise floor of selected multicouplers was found to be at or very close to the expected value of -130 dBm. This is normal a value for a CDAA site equipped 1382A multicouplers. These multicouplers were used in the high-band portion of the RFD at Northwest. Model CU-2289 multicouplers were used in the low-band portion of the RFD.

Active components in the RFD produce noise that adds to that of the primary multicouplers. Portions of the RFD employ open circuit board construction, and signal-leakage exists from adjacent beams and nearby beams into any selected beam. In addition, EMI current flowing on nearby metal objects and conductors is coupled into RFD signal paths and increases the noise floor. To understand the magnitude of these effects, the inputs to Beams 084, 156, and 252 were terminated, and the noise floor was examined. Table 2.2.2-1 provides the revised values for noise floor for the primary multicouplers and the noise added by the RFD.

Table 2.2.2-1

Noise Floor Values for Primary Multicouplers and RFD

Frequency	CU-2289	CU-1382	Beam 84	Beam 252	Beam 156
2L	3		5	6	
4L	2		5	6	
6L	2		3	5	
8L			3	6	
8H		2	4	4	4
10H		0	4	5	4
12H		0	4	5	4
14H		0	4	5	4
16H		1	4	5	3
18H		1	5	4	3
20H		2	4	4	3
22H		1	4	4	3
24H		1	4	4	3
26H		1	3	4	3
28H		0	3	3	3
30H			2	1	1

Figure 2.2.2-1 shows a visual presentation of the noise floor values listed in the above table. The visual view provides a convenient way to examine the actual operational values with respect to the nominal levels of the primary multicouplers and RFD components.

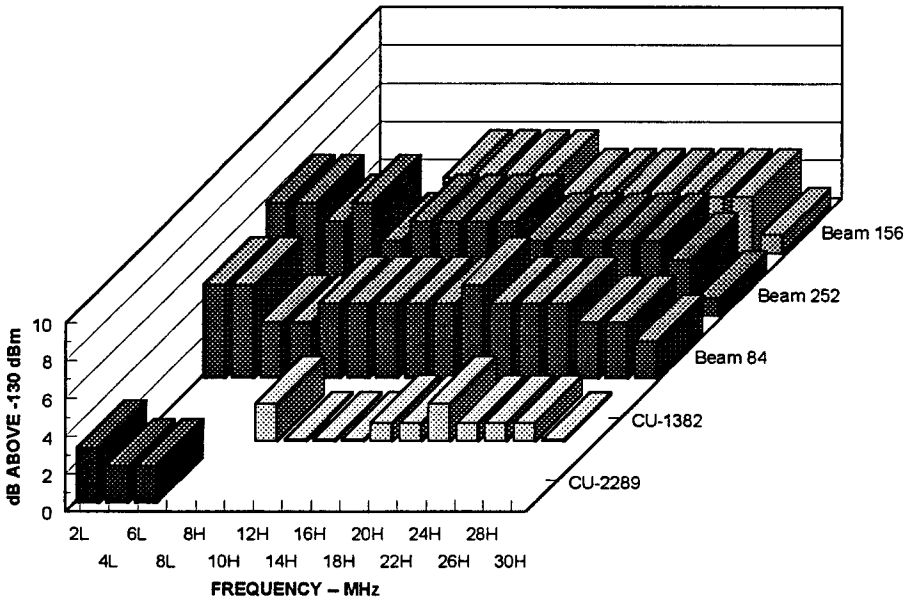

Figure 2.2.2-1

Plot of Noise Floor Values

The RFD noise floor values provided in this section are considerably different from those provided in the Quick-Look report for NW9705. An instrumentation problem was identified that gave the abnormally high values in the Quick-Look report. This caused Section 3 of this report to be revised. New signal-detection capability plots are provided in that section.

The noise floor of the Model CU-1382 Multicouplers used in the high-band portion of the RFD was slightly higher than expected although the increase is minor. No specific maintenance actions are needed for the multicouplers that are installed; although some attention might be given to noise floor of repaired and replacement multicouplers. The noise floors of the Model CU-2289 multicouplers are often slightly higher than for the Model 1382. The values measured are considered normal for that model.

RFD components increase the noise floor as shown by the increased level of noise at the output ports of ENLARGER for terminated beams 084, 252, and 156. The increase varies from about 3 to 5 dB. The variations are caused by minor resonances in the signal paths of the RFD and by the active and passive components in the various signal paths through the ENLARGER systems. Since these paths can change from time to time because of the switching arrangement of the ENLARGER system, the values of noise floor are considered nominal values. As long as the values from beam to beam are reasonably consistent, there is no reason for concern.

Ideally, RFD components would not contribute additional noise to the signal paths feeding receivers. Any increase in noise floor above that established by the primary multicouplers results in a loss of low-level signal-detection capability. Because of this, the SNEP teams pay careful attention to any increase and to the identification of its source. The increase due to RFD components is about normal for an ENLARGER-equipped site. Nevertheless, the increase is sufficient, along with signal loss due to ENLARGER, to consider feeding critical receiving systems directly from the beamformer outputs.

The beam-to-beam leakage of strong signals was as much as 30-dB above the RFD noise floor. This beam-to-beam signal leakage is not included in the noise floor values presented in Table 2.2.2-1 and Figure 2.2.2-1.

Information about the operating noise floor is provided in Section 2.2.3.

2.2.3 Operating Noise Floor

The operating noise floor was observed throughout the entire visit, and it exceeded the RFD noise floor at most times; it was especially high in the low band and in the lower portion of the high band.

Power-line noise dominated the operating noise floor during dry weather. During days with high humidity and during rainstorms, the level of power-line noise decreased slightly and noise from digital power-control devices became the dominant source. Since these two sources of noise limited the ability of the site to receive low-level signals, an attempt was made to document and understand each of the primary types of sources.

Other sources of man-made noise identified included impulsive noise from electric fences, two sources of UPS noise, motor-controller noise, and numerous erratic bursts of noise. Additional details about such sources are provided in Sections 2.3 through 2.8.

The operating noise floor was measured in hourly time increments and 2-MHz frequency increments over a 24-hour period. Table 2.2.3-1 provides the measured values for Beam 084, Table 2.2.3-2 provides the measured values for Beam 156, and Table 2.2.3-3 provides the measured values for Beam 252. The operating noise floor measurements were made at a bandwidth of 10 kHz to aid in the classification and identification of sources. The values were scaled to equivalent 3-kHz values for use later in this document.

When examining the diurnal values of noise floor, consideration must be given to the erratic and intermittent operation of many sources of man-made radio noise. This is especially the case for power-line noise where the operation of many sources is highly dependent on weather. Some sources are active during dry weather and some are active during wet weather; some sources are active all times, while others seem to be independent of any known factor. The actual noise levels can change on a much shorter time scale than the hourly increments used to obtain the data in this report. In addition, many sharp spectral peaks and nulls of each individual source of interference and noise are not shown by the rather coarse 2-MHz frequency increments of the data. It was not feasible to provide complete information about the fine-scale properties of the operating noise floor. The values shown are considered to be typical values of noise appearing at the input terminals of a receiver.

Table 2.2.3-1

Operating Noise Floor Levels for Beam 084

Local Time of Day	2 MHz	4 MHz	6 MHz	8 MHz	10 MHz	12 MHz	14 MHz	16 MHz	18 MHz	20 MHz	22 MHz	24 MHz	26 MHz	28 MHz	30 MHz
0	-87	-105	-98	-95	-95	-111	-110	-108	-111	-110	-112	-111	-112	-113	-113
1	-86	-98	-100	-97	-88	-111	-109	-108	-111	-110	-112	-111	-111	-111	-111
2	-87	-99	-100	-96	-96	-108	-111	-108	-112	-111	-112	-111	-111	-112	-112
3	-99	-99	-108	-108	-109	-111	-111	-110	-112	-111	-113	-111	-112	-112	-112
4	-100	-90	-102	-108	-108	-109	-112	-111	-115	-114	-116	-114	-117	-114	-115
5	-81	-89	-100	-99	-104	-105	-107	-108	-109	-112	-112	-104	-113	-114	-116
6	-100	-99	-106	-109	-111	-112	-112	-114	-114	-115	-114	-114	-114	-114	-114
7	-90	-103	-105	-104	-109	-113	-110	-110	-113	-112	-114	-113	-112	-113	-114
8	-102	-108	-100	-108	-98	-106	-116	-112	-114	-114	-116	-114	-112	-112	-112
9	-102	-108	-108	-112	-98	-106	-110	-110	-112	-112	-114	-114	-114	-114	-114
10	-102	-106	-108	-112	-110	-106	-110	-110	-112	-112	-114	-114	-114	-114	-114
11	-102	-100	-110	-112	-110	-114	-104	-110	-108	-112	-114	-112	-112	-112	-112
12	-103	-104	-110	-110	-110	-118	-112	-110	-112	-112	-115	-114	-114	-114	-114
13	-98	-103	-110	-109	-110	-110	-110	-110	-111	-114	-112	-116	-112	-114	-114
14	-98	-102	-109	-109	-111	-115	-116	-111	-112	-112	-114	-114	-114	-114	-112
15	-98	-100	-110	-110	-108	-112	-110	-112	-114	-114	-116	-114	-114	-114	-113
16	-102	-103	-108	-111	-109	-109	-111	-110	-114	-113	-116	-114	-114	-114	-113
17	-102	-101	-106	-109	-108	-108	-110	-110	-115	-113	-114	-113	-112	-112	-112
18	-104	-100	-109	-109	-108	-107	-106	-110	-114	-114	-115	-113	-113	-113	-113
19	-101	-98	-104	-106	-102	-108	-110	-110	-114	-112	-115	-114	-114	-113	-112
20	-102	-98	-106	-98	-96	-108	-108	-108	-114	-112	-114	-114	-114	-114	-114
21	-90	-94	-96	-94	-94	-108	-106	-106	-106	-112	-114	-114	-114	-114	-116
22	-90	-94	-96	-96	-94	-110	-110	-108	-106	-112	-114	-114	-114	-114	-114
23	-86	-94	-96	-94	-94	-110	-114	-108	-112	-112	-114	-114	-114	-114	-114

Table 2.2.3-2

Operating Noise Floor Levels for Beam 156

Local Time of Day	2 MHz	4 MHz	6 MHz	8 MHz	10 MHz	12 MHz	14 MHz	16 MHz	18 MHz	20 MHz	22 MHz	24 MHz	26 MHz	28 MHz	30 MHz
0	-80	-88	-97	-87	-85	-108	-110	-111	-112	-111	-112	-112	-112	-112	-112
1	-78	-88	-90	-87	-87	-102	-110	-109	-111	-110	-113	-111	-111	-111	-111
2	-80	-88	-99	-87	-86	-108	-109	-106	-110	-109	-112	-110	-110	-111	-111
3	-99	-98	-109	-108	-101	-111	-110	-110	-111	-110	-113	-112	-111	-112	-112
4	-99	-90	-98	-107	-100	-106	-108	-108	-109	-109	-110	-112	-114	-114	-115
5	-99	-88	-86	-94	-103	-106	-108	-109	-110	-110	-112	-113	-113	-114	-115
6	-99	-96	-96	-106	-105	-108	-110	-109	-113	-112	-115	-113	-112	-113	-114
7	-101	-104	-102	-107	-107	-108	-109	-110	-112	-112	-115	-113	-113	-113	-114
8	-98	-98	-102	-100	-102	-108	-112	-116	-110	-112	-116	-114	-114	-112	-112
9	-102	-102	-108	-112	-110	-110	-112	-112	-112	-112	-112	-112	-114	-114	-114
10	-102	-106	-110	-112	-110	-108	-112	-112	-112	-112	-112	-112	-112	-112	-112
11	-102	-106	-110	-112	-110	-110	-112	-112	-114	-113	-115	-114	-114	-114	-114
12	-102	-106	-110	-112	-110	-110	-117	-112	-114	-113	-115	-114	-114	-114	-114
13	-98	-108	-109	-110	-112	-112	-113	-112	-114	-112	-115	-114	-113	-114	-114
14	-100	-107	-110	-110	-110	-111	-113	-112	-112	-110	-115	-114	-114	-114	-114
15	-98	-102	-109	-109	-110	-110	-112	-111	-113	-112	-115	-114	-112	-114	-114
16	-100	-108	-112	-108	-109	-110	-110	-110	-108	-107	-114	-113	-114	-112	-113
17	-102	-108	-111	-112	-109	-109	-112	-111	-114	-110	-114	-112	-112	-113	-112
18	-105	-99	-111	-108	-103	-106	-110	-110	-113	-112	-114	-114	-113	-114	-113
19	-101	-96	-104	-108	-103	-98	-109	-108	-112	-110	-115	-114	-113	-114	-113
20	-98	-88	-100	-90	-86	-104	-108	-108	-110	-112	-116	-116	-116	-116	-116
21	-86	-88	-100	-88	-88	-104	-106	-108	-112	-112	-114	-114	-116	-116	-116
22	-86	-86	-94	-88	-88	-106	-110	-110	-112	-114	-114	-114	-116	-116	-116
23	-82	-88	-96	-88	-86	-108	-112	-108	-110	-112	-114	-114	-116	-116	-116

Table 2.2.3-3

Operating Noise Floor Levels for Beam 252

Local Time of Day	2 MHz	4 MHz	6 MHz	8 MHz	10 MHz	12 MHz	14 MHz	16 MHz	18 MHz	20 MHz	22 MHz	24 MHz	26 MHz	28 MHz	30 MHz
0	-80	-78	-98	-90	-78	-110	-111	-111	-112	-112	-113	-112	-113	-112	-112
1	-92	-85	-100	-96	-102	-110	-111	-111	-112	-111	-113	-111	-111	-111	-112
2	-92	-88	-99	-96	-108	-108	-111	-111	-110	-111	-112	-112	-112	-112	-112
3	-81	-80	-100	-88	-108	-112	-111	111	-113	-111	-113	-112	-112	-112	-112
4	-102	-88	-95	-89	-108	-109	-110	-110	-112	-113	-112	-112	-114	-114	-115
5	-84	-79	-86	-95	-80	-101	-108	-109	-109	-111	-112	-112	-113	-114	-115
6	-110	-90	-88	-99	-102	-109	-110	-110	-112	-112	-115	-114	-114	-114	-114
7	-110	-94	-96	-96	-93	-100	-98	-109	-109	-110	-110	-112	-113	-112	-112
8	-98	-96	-92	-104	-98	-102	-108	-108	-110	-110	-114	-112	-114	-114	-114
9	-110	-110	-110	-104	-110	-98	-104	-98	-108	-108	-114	-112	-114	-114	-114
10	-110	-102	-108	-108	-104	-106	-104	-106	-108	-108	-112	-112	-112	-112	-112
11	-110	-106	-108	-110	-104	-106	-108	-108	-108	-110	-112	-112	-112	-112	-112
12	-101	-108	-108	-108	-108	-110	-110	-110	-113	-112	-116	-114	-114	-114	-114
13	-106	-108	-108	-108	-106	-107	-108	-108	-106	-111	-115	-116	-114	-114	-113
14	-108	-107	-110	-106	-105	-107	-110	-110	-103	-101	-114	-114	-114	-114	-114
15	-98	-105	-108	-106	-104	-107	-109	-109	-110	-110	-114	-114	-114	-114	-114
16	-109	-106	-108	-104	-103	-105	-106	-107	-108	-107	-112	-113	-114	-113	-114
17	-108	-102	-103	-108	-100	-104	-107	-104	-110	-109	-114	-113	-114	-113	-111
18	-110	-95	-104	-106	-98	-102	-106	-106	-105	-109	-114	-113	-113	-112	-112
19	-103	-96	-98	-98	-98	-100	-104	-104	-108	-108	-112	-113	-114	-114	-113
20	-100	-90	-100	-98	-96	-104	-102	-102	-104	-108	-114	-114	-114	-114	-114
21	-98	-94	-96	-94	-94	-98	-100	-98	-98	-110	-114	-114	-114	-114	-114
22	-96	-86	-82	-92	-96	-106	-106	-98	-112	-114	-116	-116	-114	-116	-114
23	-94	-86	-88	-94	-102	-108	-108	-106	-114	-114	-116	-116	-116	-116	-116

The data in Tables 2.2.3-1 through 2.2.3-3 was taken with a gaussian-shaped measurement bandwidth of 10 kHz. The data was converted to 3-kHz gaussian-shaped bandwidth values and in terms of dB above the noise floor of the primary multicouplers. A graphic presentation of the operating noise floor for Beam 084 is found in Figure 2.2.3-1 and provides an excellent understanding of the time-changing and erratic values of the operating noise floor presented to receivers using Beam 084.

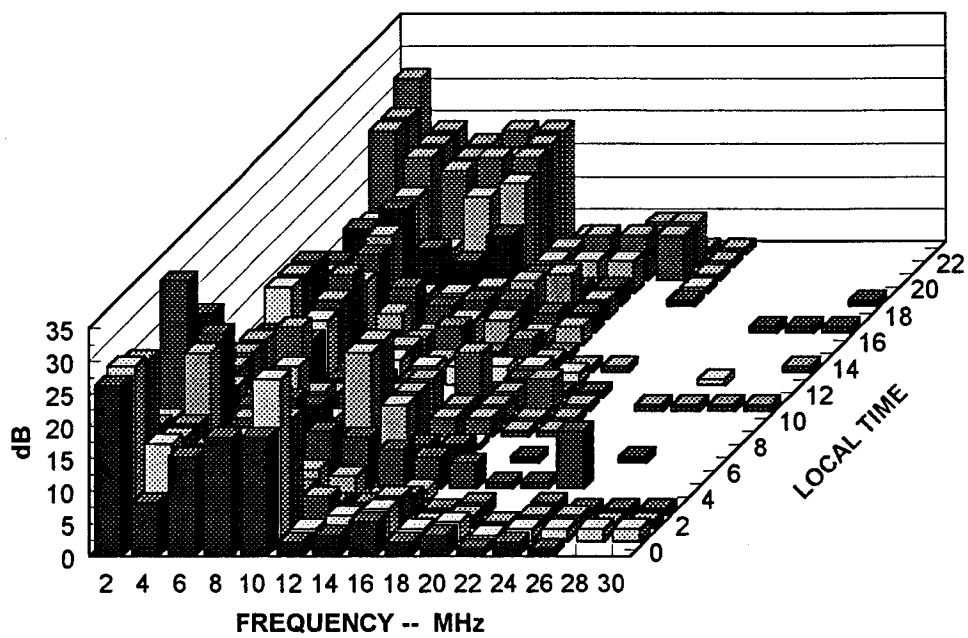

Figure 2.2.3-1

Graphic Presentation of the Operating Noise Floor for Beam 084

Figure 2.2.3-2 provides a similar graphic presentation of the operating noise floor for Beam 156, and Figure 2.2.3-3 shows the operating noise floor for Beam 288. Again, the time-varying and erratic nature of the noise presented to receivers using these beams is clearly shown.

The operating noise floor consisted of noise from several sources. Typical sources encountered and identified included power-line noise, variable-speed motor-controller noise, noise from two UPS systems, and noise from a diesel-generator control device. Other erratic and intermittent noise from unknown sources is also included in the data.

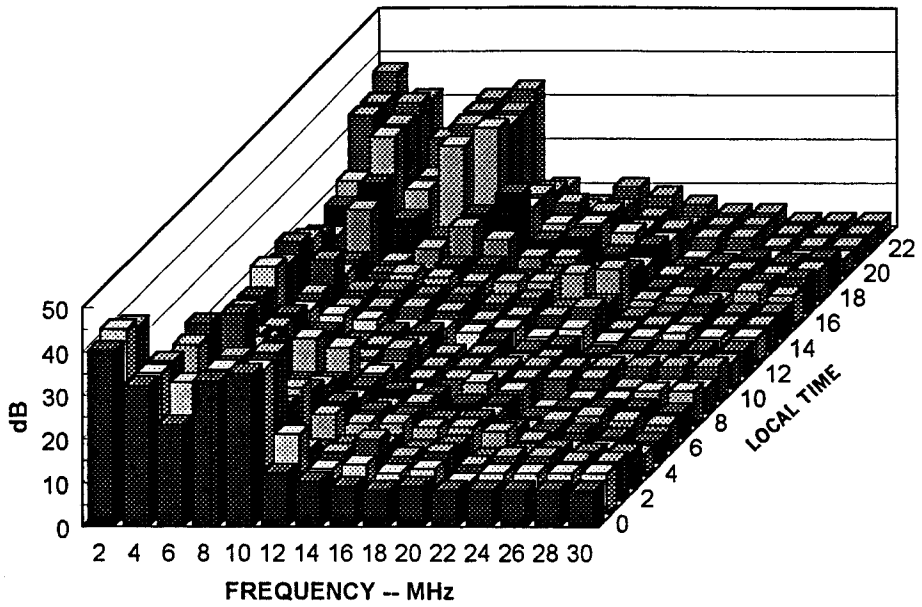

Figure 2.2.3-2

Graphic Presentation of the Operating Noise Floor for Beam 156

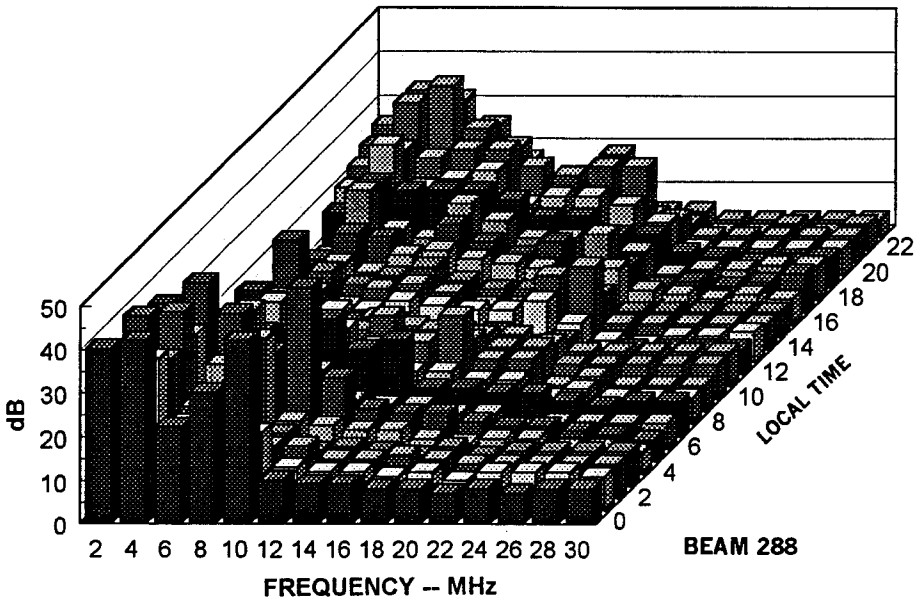

Figure 2.2.3-3

Graphic Presentation of the Operating Noise Floor for Beam 288

Of special interest is that the noise at the low end of the HF band peaked in amplitude around midnight. This implies that intermodulation noise from overloaded and saturated RFD components was also included in the operating noise floor. The mix of sources contributed to the operating noise floor, and each source needs to be tracked down and eliminated.

The observations of noise in the three beams sheds considerable light on the statistical nature of the operating noise floor. While the noise might be considered frequency flat over very narrow portions of the HF band, it is not frequency flat over the bandwidths of some of the newer kinds of wide-band signals appearing in the HF band. In addition, the erratic temporal properties of the noise suggest that it might not fit the statistical gaussian classification typically used in the analysis of the detection of communications signals.

The measurement intervals of time (1 hour) and frequency (2 MHz) of the data used in this report were dictated by instrumentation and operator-time limitations. The data strongly suggest that the time and frequency intervals of the measured data need to be significantly decreased before one can fully understand the erratic nature and time-varying properties of the operating noise floor. While the team has obtained noise data at finer time and frequency intervals over small portions of the HF band, it was not possible to make this measurement during the NW9705 visit.

2.3 POWER LINE NOISE

Power-line noise was recognized as a major problem at NSGA Northwest by an early SNEP team in January 1978.[1] A detailed survey of sources of power-line noise was completed 10-years later in January 1988.[2] Additional efforts were undertaken during subsequent years to reduce the impact of power-line noise on the reception of signals at the site, but formal reports were not completed describing progress. Available notes and trip reports on these efforts were reviewed by the NW9705 team members prior to this visit, and the available data is summarized in Appendix B. Known information about sources was transcribed onto standard source-identification forms, and GPS pole-location information was added to the forms along with a summary of the current status of each source. Transmission-line sources are also included in Appendix B. While several transmission-line sources were visited during the NW9705 survey, a few were not because unfavorable terrain conditions and excessive surface water did not permit team members to walk the complete transmission line right of way.

Of high interest is that all distribution-line sources listed in Appendix B and reviewed by the NW9705 team were noise quiet. Most of these poles had been modified by the utility operating the lines in accordance with the noise-free techniques described in the SNEP team Power-Line Noise Mitigation Handbook.[3] It is apparent that the primary sources of power-line noise affecting the operation of the Northwest CDAA site have been eliminated. Only the lower-level sources were present at the time of the NW9705 survey.

While a comprehensive survey of all remaining sources of power-line noise could not be accomplished during this visit, several active sources were noted during the internal noise investigation. Six of these sources were located. Appendix C provides data sheets for the sources identified during the NW9705 survey.

---

1 Wilbur R. Vincent and Gene Cummins, *Radio Noise Measurements at Naval Security Group Activity, Northwest, Chesapeake, Virginia*, Technical Report, January 1978.

2 Wilbur R. Vincent, *Signal-to-Noise Enhancement at the Northwest CDAA*, Technical Report prepared for Melpar Division, E-Systems, Falls Church, VA, January 1988.

3 Wilbur R. Vincent and George F. Munsch, *Signal-to-Noise Enhancement Program Power-Line Noise Mitigation Handbook*, 4th edition, Prepared for COMNAVSECGRU, January 1997.

Figure 2.3-1 is a map of the area surrounding the site. It shows the location of the distribution-line sources listed in Appendices B and C. The sources shown as solid dots are those from Appendix B. These sources are shown for reference only since they were noise-quiet during the NW9705 visit. The sources containing a circle around the solid dot are new sources identified during the NW9705 visit. Many additional sources affecting the operational the site were not located during the NW9705 visit because of the lack of sufficient time to conduct a comprehensive internal-external source-location effort. Inclement weather further reduced the time available for source-location work.

Examples of the properties of power-line noise noted during the NW9705 survey are provided in this section. The record of the temporal and spectral properties of the noise provided in these examples will be useful during future mitigation actions. Figure 2.3-2 (970429 1608) shows the fine-scale temporal structure of a single source of noise noted at 4.4 MHz in Beam LBM192. The source contained groups of three to four impulses of noise spaced at intervals of 8.33 ms. The impulses within each group are spaced about 1-ms apart. The impulse-to-impulse spacing varies slightly since the impulse generation mechanism of the source is not perfectly stable. This spacing is designated as "wide spacing" in the source records to distinguish it from many other sources with much narrower impulse-to-impulse spacing. The duration of each impulse is very short, less than the approximately 40-μs time resolution of the data shown in the figure. The impulse amplitude as measured in a 30-kHz bandwidth is about -100 dBm. This reduces to an amplitude of about -120 dBm for a 3-kHz receiver bandwidth.

Figure 2.3.3 (970429 1556) is another example of power-line noise received in Beam LBM024 and shows three distinct sources. The time-history view shows an intermittent source of overlapping pulses occurring at intervals of about 0.9 second and a group-to-group spacing of 8.33 milliseconds. A second source with characteristics similar to those shown in the previous figure is present. The third source produced the wide-spaced impulses also present in the time-history view. The relative amplitudes of these three sources are shown in the upper amplitude-vs.-frequency view. The highest level source is about -90 dBm in a 30-kHz wide bandwidth or about -110 dBm in a 3-kHz bandwidth. The groups of the first two sources are spaced 8.33-ms apart. The large spacing of the third source is typical of hardware-related sources that produce individual impulses which are synchronized to the line frequency.

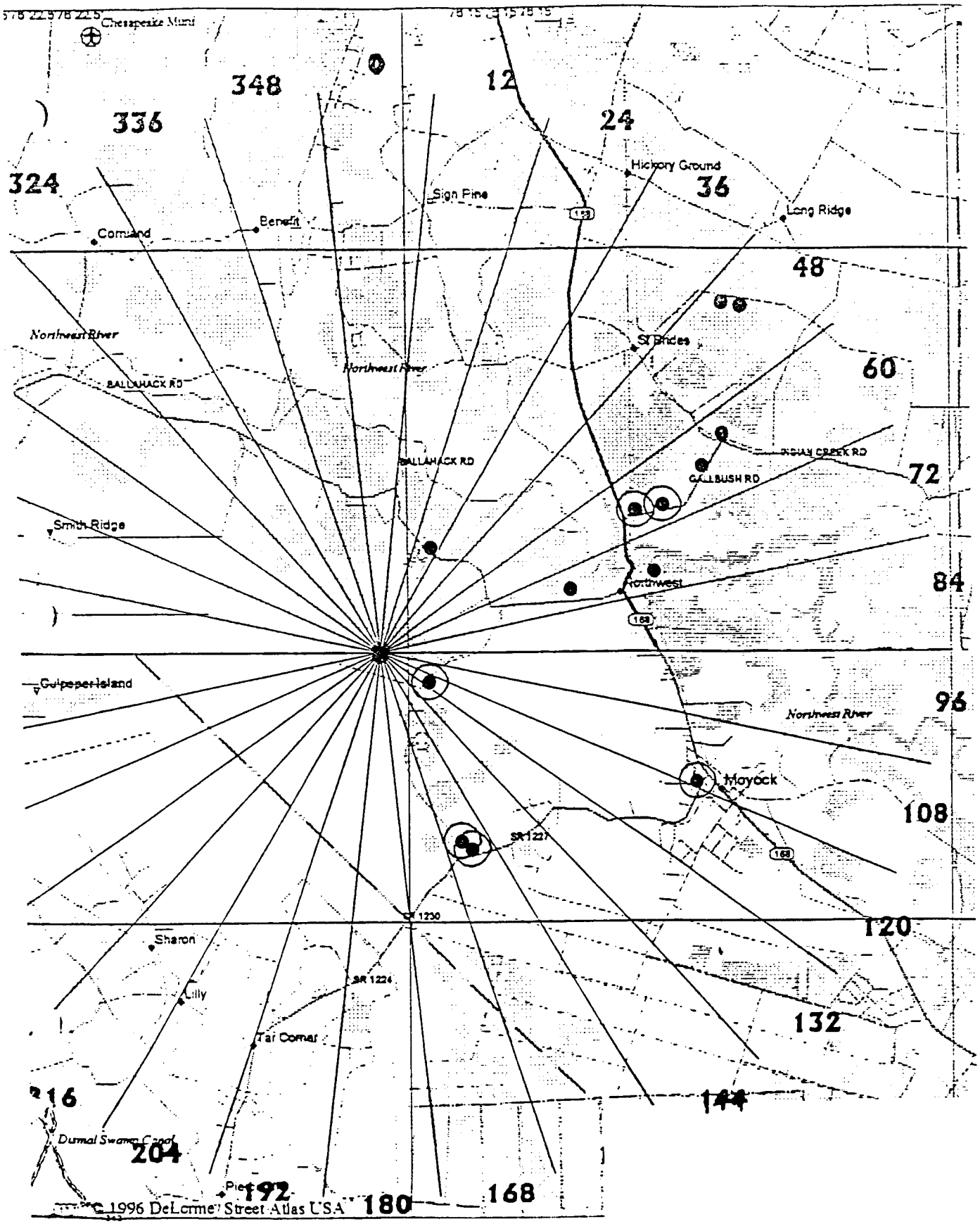

Figure 2.3-1

Map Showing Location of Sources of Power-Line Noise

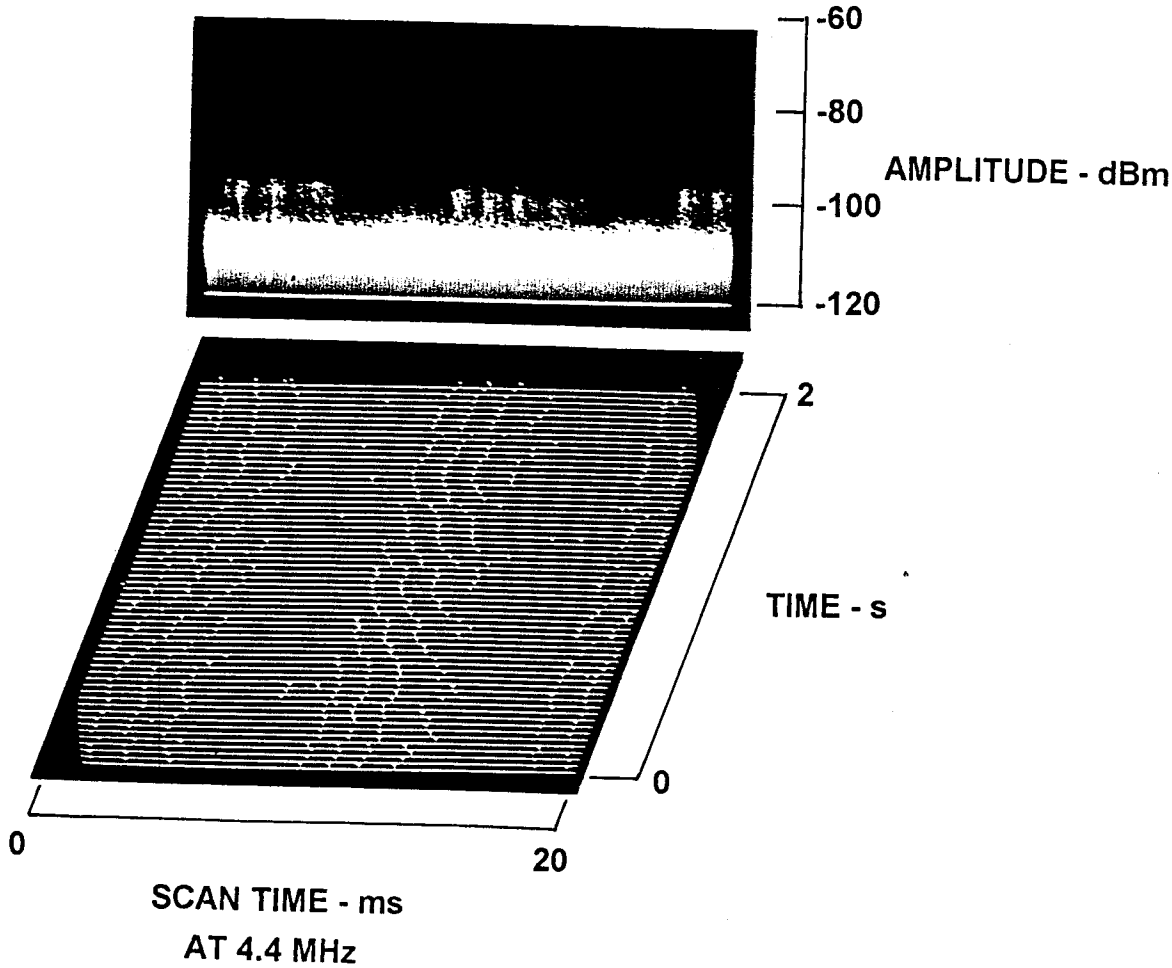

970429 1608
NW, RFD, LBM 192
4.4 MHz, 0, 30 kHz, 20 ms LS
BPF 1, +20, 0, -20

Figure 2.3-2

Fine-Scale Temporal Structure of a Single Source of Power-Line Noise

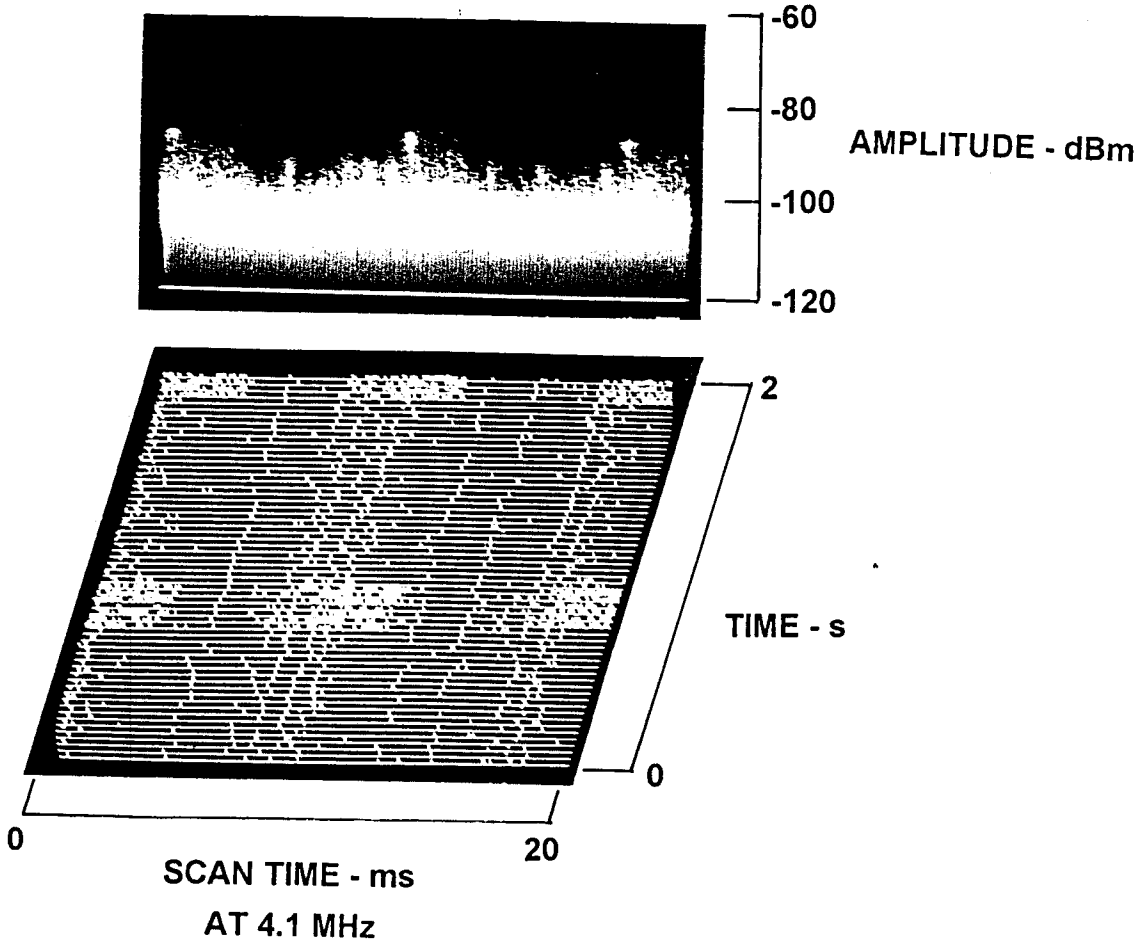

970429 1556
NW, RFD, LBM 024
4.1 MHz, 0, 30 kHz, 20 ms LS
BPF 1, +20, 0, -20

Figure 2.3-3

Fine-Scale Temporal Structure of Three Sources of Power-Line Noise

This is a typical view of power-line noise observed at the input terminals of a site's receiver. The instrumentation operator must distinguish the noise produced by one source from the others, recognize each pattern, measure its amplitude, understand its behavior with time, relate each temporal structure to a specific type of source, and obtain a bearing to each source.

Figure 2.3-4 (970428 1030) shows still another typical noise found at the input terminals of a receiver. A single source of power-line noise produced the high-amplitude cluster of impulses near the left edge of the scan-time scale and a second cluster partly shown at the right edge of the time scale. The clusters are spaced 16.6-ms apart, indicating that the source produced noise only on either the negative or the positive portion of the line-voltage waveform. The amplitude of these two clusters is about -81 dBm in a 30-kHz bandwidth (or about -99 dBm in a 3-kHz bandwidth). This is higher in amplitude than the average amplitude of most signals of interest, hence the noise is of concern.

Two additional kinds of noise are shown in Figure 2.3-4. Two discrete temporal components are shown near the center of the horizontal scan-time scale. These are impulses from the site's UPS and they are discussed in more detail later in this report (see Section 2.5). In addition, low-level and closely-spaced impulses that are not synchronized with the line frequency are shown in the time-history view. These impulses are from a variable-speed motor controller;, interference from this source is also discussed later in this report (see Section 2.4). This is a typical view of the mixture of types of noise often presented to the instrumentation operator who must be able to sort power-line noise from many other kinds of radio interference and deal with each on an individual basis. This process also suggests that other lower-level sources of interference probably exist that are covered by the higher-level sources shown.

An ongoing comprehensive mitigation effort is required to further decrease the number of sources of power-line noise and to decrease their impact on the reception of signals. All future mitigation work on power lines should be accomplished in strict accordance with the procedures in Reference 3 and in cooperation with the public utilities operating the power lines.

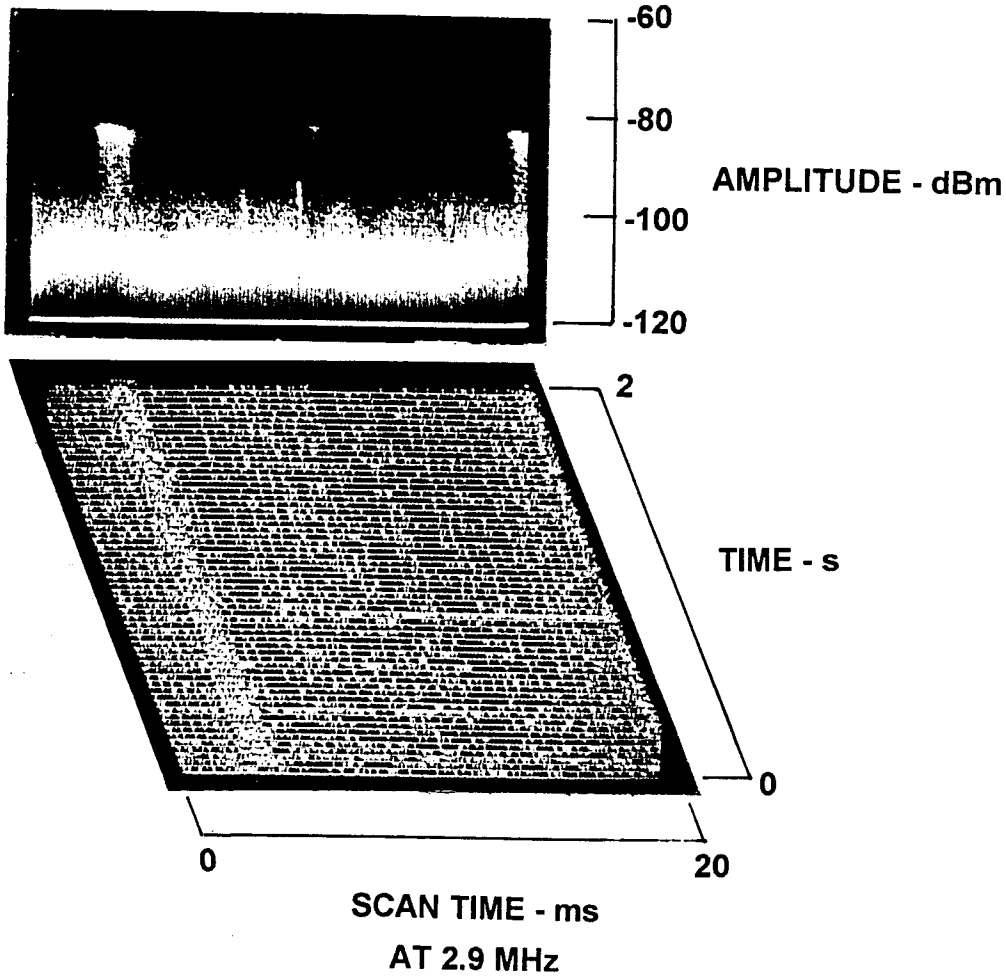

970428 1030
NW, RFD, LBM048
2.9 MHz, 0, 30 kHz, 20 ms LS
BPF-1, +20, 0, -20

Figure 2.3-4

Combination of Noise from a Power-Line and a Power-Control Device

2.4 MOTOR-CONTROLLER INTERFERENCE

During the internal noise survey, considerable radio interference from digital power-control devices was noted. This interference was unusually strong in Beams A024 and A036. The primary source was traced to a digital, variable-speed, induction-motor controller located in Room 191 of the CDAA Operations Building. The digital device controlled the air flow in the air-conditioning system for a portion of the Operations Building. The controller injected excessive levels of EMI current onto all power conductors and conduits in the vicinity of the controller and onto power conductors and conduits providing power to trailers outside the building. EMI current flowing on the conduits and power wires to the trailers was conducted onto the outside metal surface of the trailers. Radiation from the complex array of conductors and trailers was sufficiently strong to be received as radio interference by the CDAA elements.

Figure 2.4-1 (970505 1307) shows an example of the change in the noise received by Beam A024 as the motor controller was operated and then turned off. The amplitude of the noise floor produced by the air-handler controller was about -100 dBm in a 10-kHz bandwidth. The equivalent level in a 3-kHz bandwidth is about -105 dBm. The upper half of the time-history view shows the coarse-scale temporal structure of the motor-controller noise. The data was obtained with the scanning process of the receiver synchronized to the power-line frequency. The slanting lines across the view indicate that the impulsive portions of the noise generated by the motor controller were not synchronized with the power-line frequency. When the motor controller was turned off, the operating noise floor decreased to the amplitude of noise from other lower-level sources.

Signals below -105 dBm could not be received over the band from 2 to about 4 MHz. The motor-controller noise decreased as frequency was increased and became less objectionable at higher frequencies. It fell below other sources of noise at about 4.5 MHz.

Since the motor-controller noise was a significant factor affecting the reception of signals, it was further investigated. Instrumentation to measure conducted EMI current generated by the motor controller was moved to Room 191, the location of the controller and the air-handler fan with its variable-speed motor. The label on the controller unit indicated that it is capable of providing more than 30 amperes of three-phase current at 208 volts.

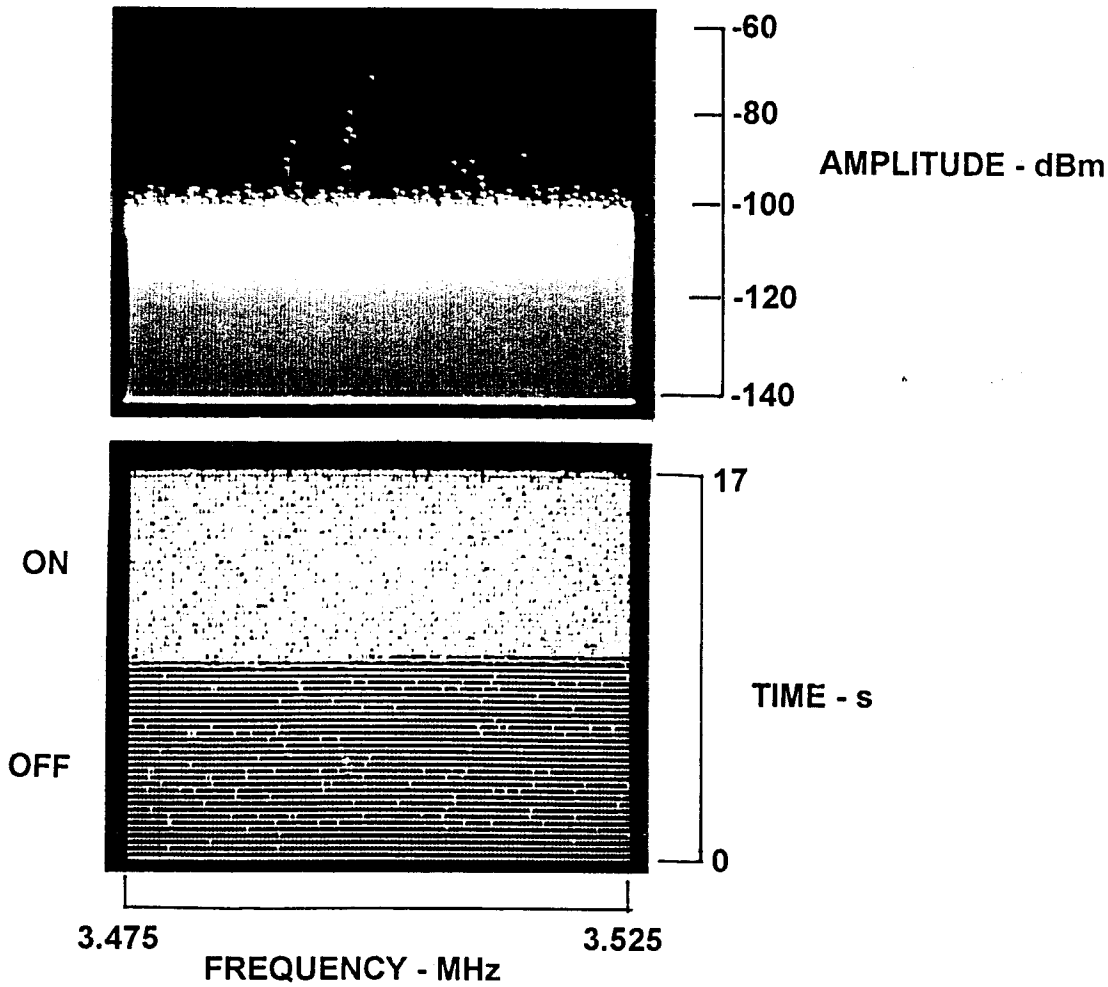

970505 1307
NW, RFD, LBM 024
3.5 MHz, 50 kHz, 10 kHz, 200 ms LS
BPF (2-8), +20, 0, -40

Figure 2.4-1

Interference from Variable-Speed Motor Controller for Air Handler

Verification that conductors in the vicinity of the motor controller radiate excessive levels of interference was obtained by placing a test antenna at the doorway to Room 191 and employing the SNEP instrumentation to observe the radiated interference. The top photograph of Figure 2.4-2 (970505 0925) shows the coarse-scale spectral shape of the radiated interference over the frequency range of about 1 MHz to 50 MHz. Peaks and nulls can be seen in the spectral data. Significant levels of interference were radiated from the vicinity of the motor controller at frequencies up to 30 MHz. The amplitude of noise below 1 MHz was suppressed by the bandpass characteristics of the instrumentation. The coarse-scale temporal structure of the interference can be seen in the time-history view.

Figure 2.4-3 (970505 0942) shows the fine-scale temporal structure at a frequency of 18 MHz. Closely-spaced groups of impulses of noise are shown. The impulse occurrence rate was not synchronized with the line frequency as indicated by the slanting lines across the time-history view. The occurrence rate was established by the motor controller to operate the fan motor at a desired speed. While the test antenna was not calibrated for Figures 2.4-2 and 2.4-3, the high amplitude of the data indicate that the interference level was very high near the outside door for Room 191.

To better understand the radiation mechanisms involved in the motor-controller interference, the EMI current injected onto several nearby conductors was examined. The power panel supplying 208-V, three-phase power to the motor controller was opened, and a Fischer Model F-70 Current Clamp was placed around the three-phase conductors leading to the motor controller. Figure 2.4-4 (970505 1105) shows the common-mode current flowing on these conductors. The controller injects significant levels of current back into the building's power conductors at frequencies from low-order harmonics of the power frequency up to well above the upper-frequency limit of the data of 20 MHz. The peak current is about 10 mA at a frequency near 6 MHz. This is equivalent to the current injected into an antenna by a low-power transmitter used for long-distance communications.

Next, the current on the ground wire in the power panel was examined. Figure 2.4-5 (970505 1106) shows the ground current vs. frequency. The ground current at high frequencies was somewhat lower than the phase current but still significant. A peak was again noted near 6 MHz at a level of about 2 mA.

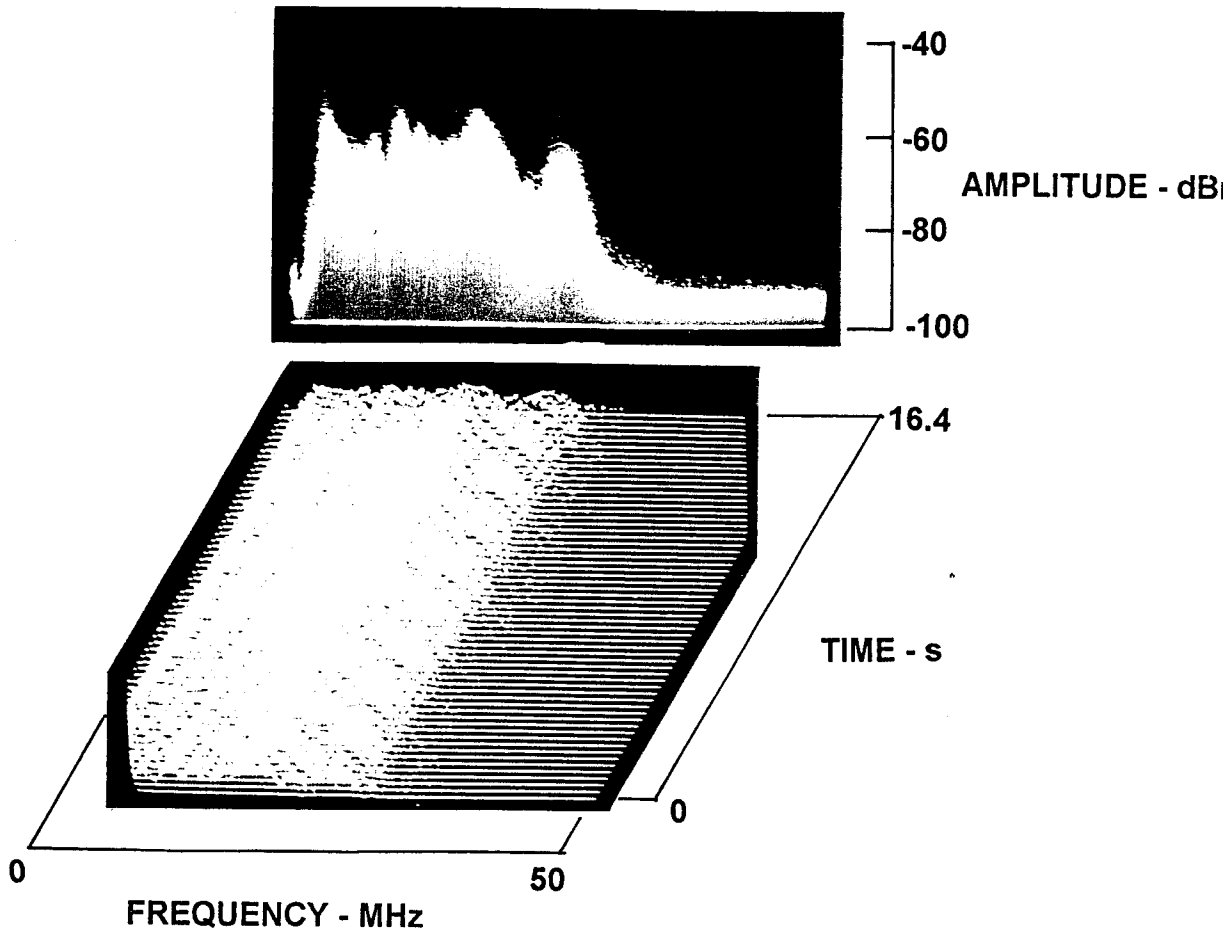

970505 0925
NW, Rm 191, Create Outside Door
25 MHz, 50 MHz, 30 kHz, 200 ms
Create, 0, -20

Figure 2.4-2

Coarse-Scale Spectral and Temporal Structure of Interference Radiated from the Motor Controller

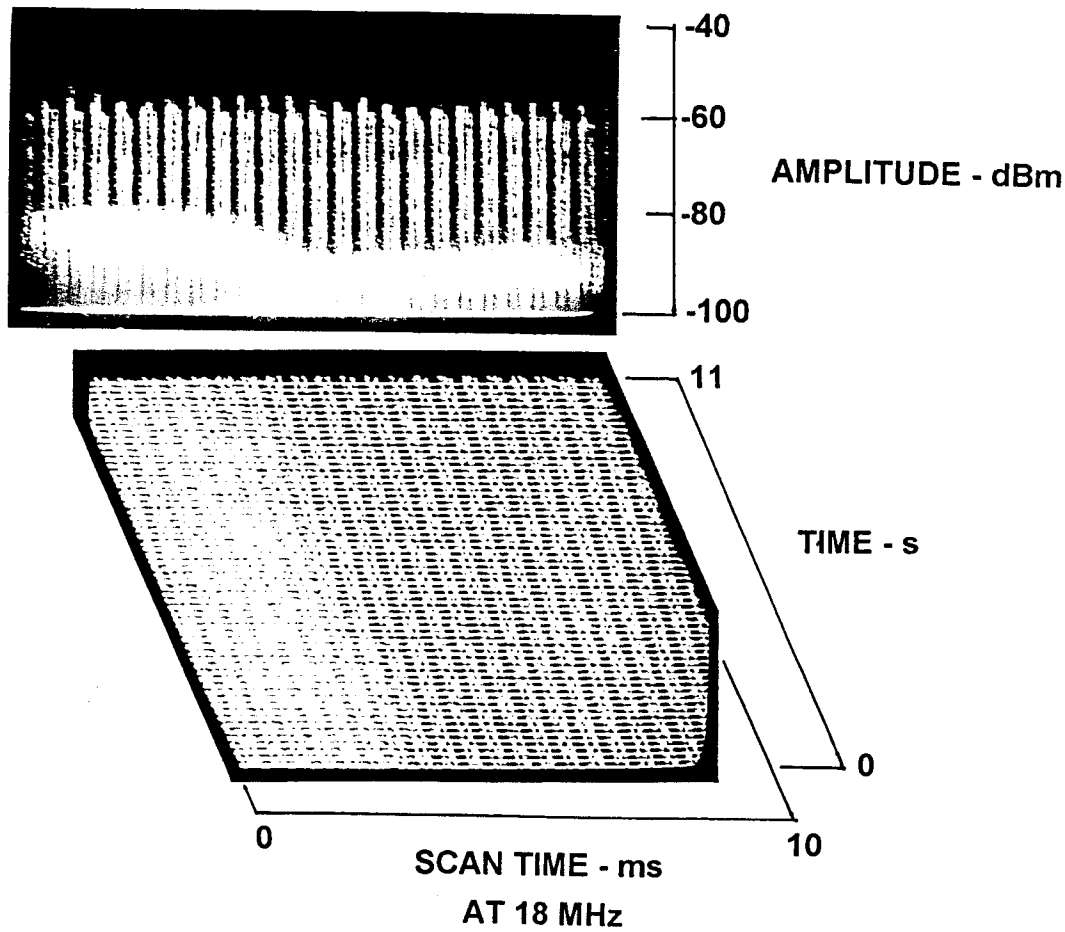

970505 0942
NW, Rm 191
18 MHz, 0, 30 kHz, 10 ms LS
Create, 0, -20

Figure 2.4-3

Fine-Scale Temporal Structure of Interference Radiated from the Motor Controller

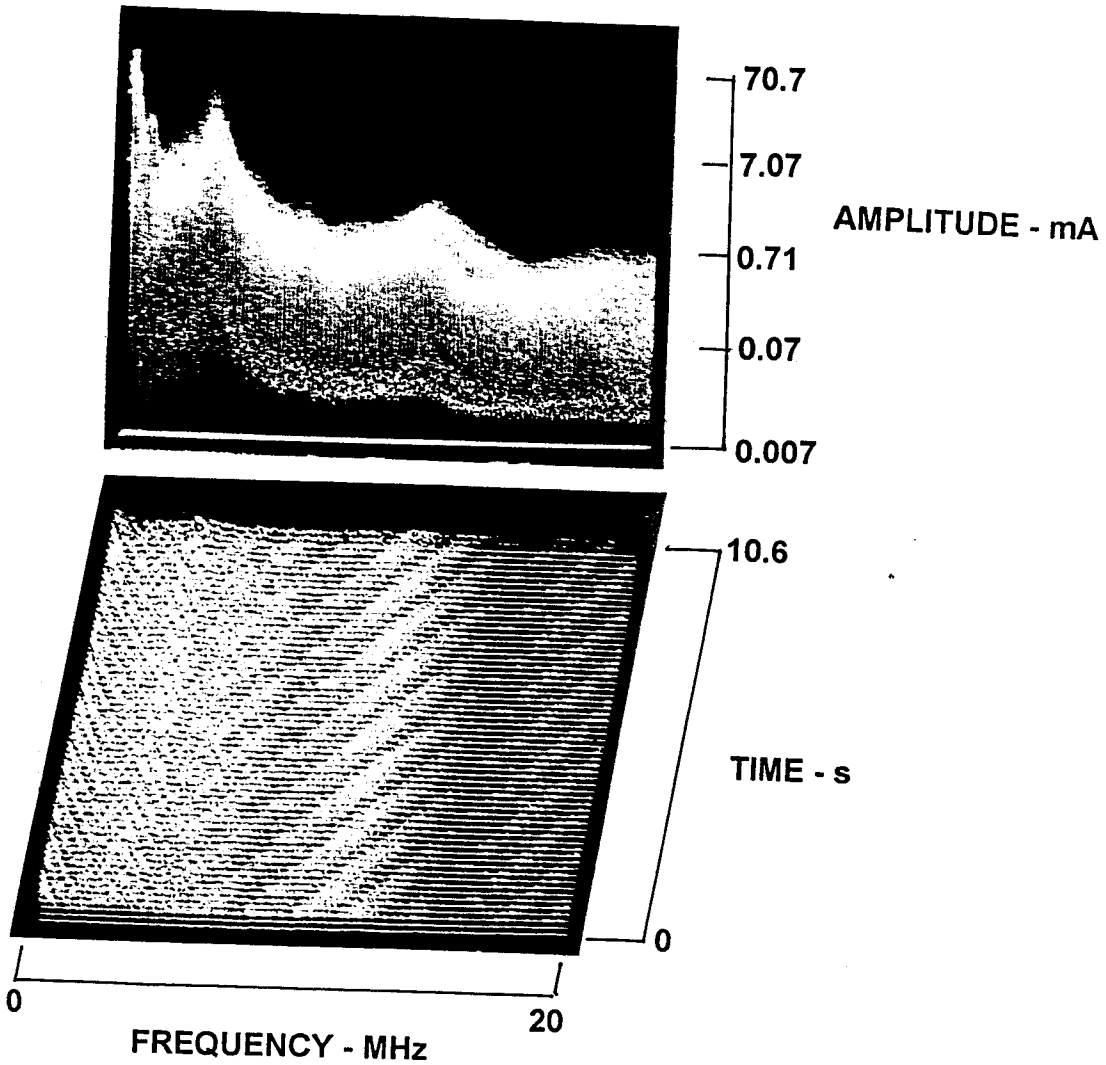

970505 1105
NW, Rm 191, Common Mode of
all 3 phases in Panel N-191-8-191B
10 MHz, 20 MHz, 30 kHz, 100 ms
F-70, -10, -10

Figure 2.4-4

Common-Mode EMI Current Injected Back onto the Phase Conductors in the Power Panel

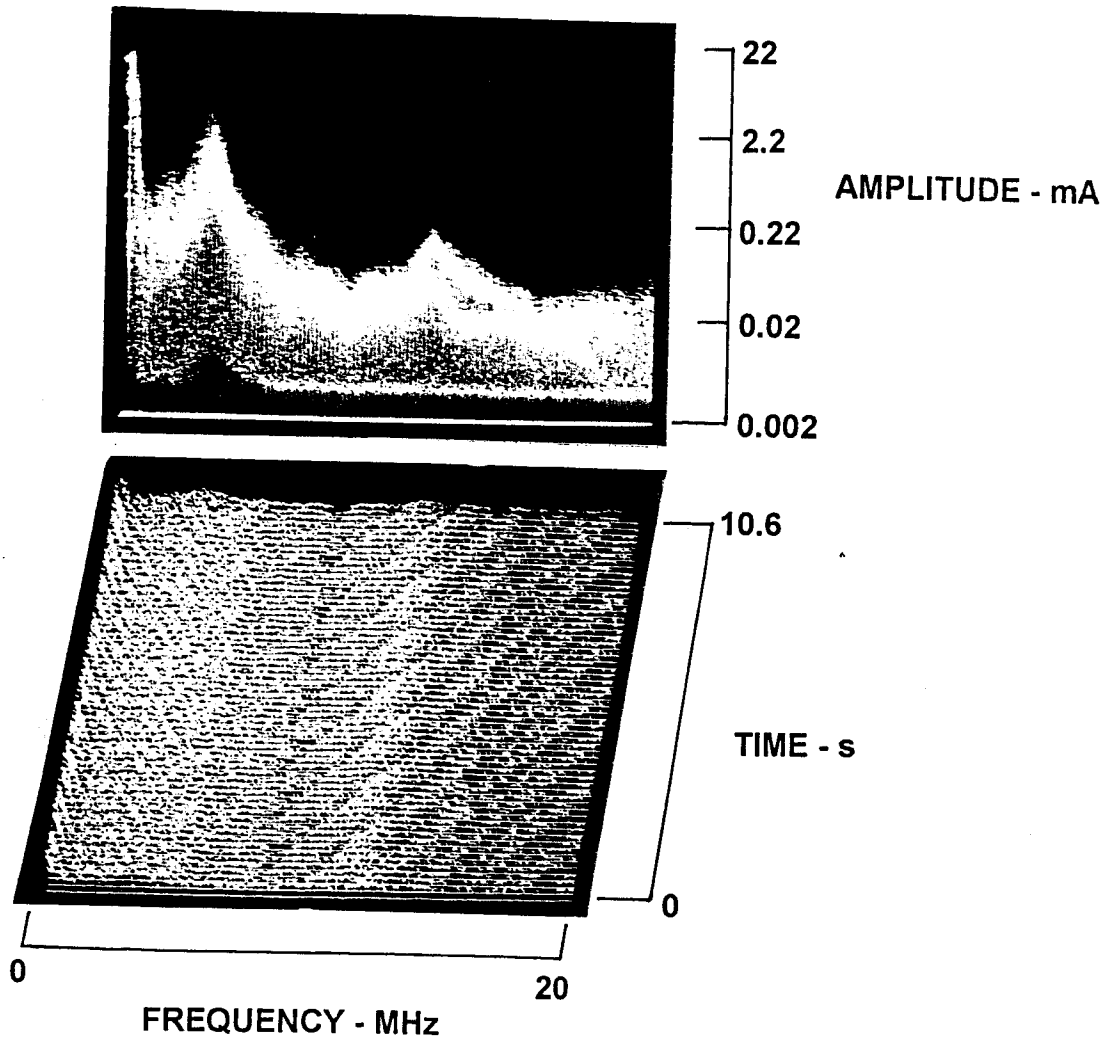

970505 1106
NW, Rm 191, Ground Conductor
in Panel N-191-8-191B
10 MHz, 20 MHz, 30 kHz, 100 ms
F-70, 0, -20

Figure 2.4-5

EMI Current Injected into the Ground Conductor in the Power Panel

The EMI current flowing on the conduit running from the power panel in Room 191 to the motor-controller unit was examined. A Model F-70 Current Clamp was placed around the conduit at a location near the motor-controller housing. Figure 2.4-6 (970505 1018) shows that EMI current flowing on the conduit is similar in spectral shape and only slightly lower in amplitude than common-mode current flowing on the phase conductors. The peak current is about 7 mA (compared to 10 mA on the phase conductors) and also at a frequency near 6 MHz. This shows that the configuration of the metal power conduits and the related power panels do not provide effective shielding for high-frequency EMI current.

Power to operate the electronics in the motor controller was provided by a separate 120-V, single-phase line running in another conduit from the power panel to the motor controller. EMI current on this conduit was also measured; the F-70 Current Probe was placed around the 120-V conduit near the motor-controller unit. Figure 2.4-7 (970505 1025) shows the high-frequency EMI current flowing in the outside surface of the conduit. The maximum EMI current flowing on this conductor also occurred at a frequency near 6 MHz. The amplitude at this frequency was about 5 mA, only slightly less than the EMI current flowing on the 208-V, three-phase conduit.

Another section of conduit ran from the motor controller to the sheet-metal enclosure housing the fan and its motor. The Model F-70 Current Clamp was placed around this conduit at a location near the controller to determine the level of current injected onto that conductor and onto the sheet-metal fan and motor enclosure. Figure 2.4-8 (970505 1015) shows the high-frequency EMI current injected onto the outer surface of the conduit. Again, the maximum current occurred near 6 MHz at a level of about 6 mA. Significant levels of EMI current were found at frequencies up to 20 MHz.

Crude measurements with a hand-held HF radio (Sony Model 2010) indicated that EMI current was flowing on the shield of the cable providing power to the Coyote van located outside the Operations Building. A large breaker panel adjacent to Room 191 was the source of power for both the Coyote van and the motor controller. It was suspected that EMI current was conducted through the power system and onto the Coyote van cable. The F-70 Current Clamp was used to measure the shield current on this cable.

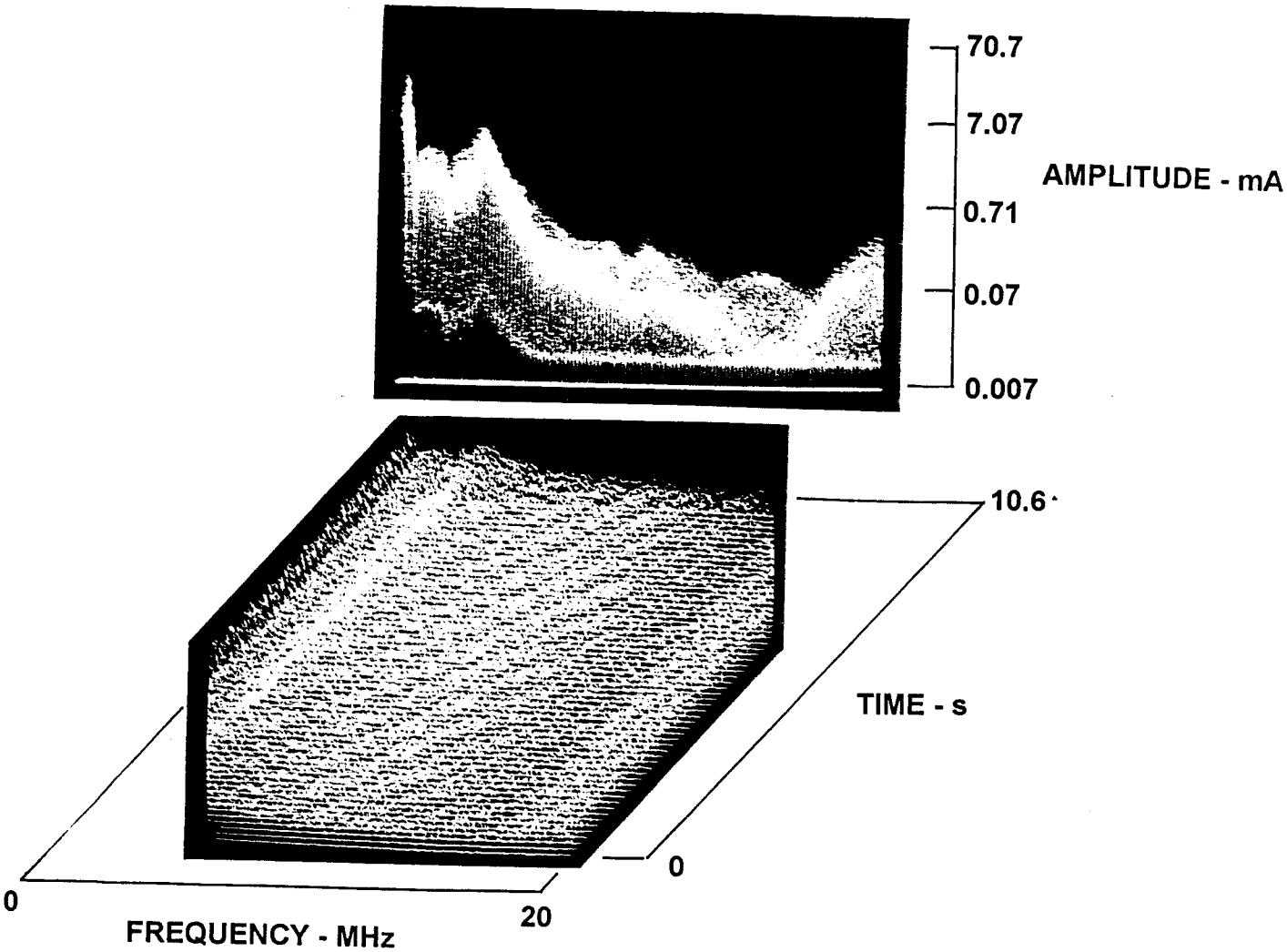

970505 1018
NW, Rm 191, Input Conduit
Motor Controller (208 V, 3 phase)
10 MHz, 20 MHz, 30 kHz, 100 ms
F-70, -10, -10

Figure 2.4-6

EMI Current on the 208-V, 3-Phase Power Conduit for the Motor Controller

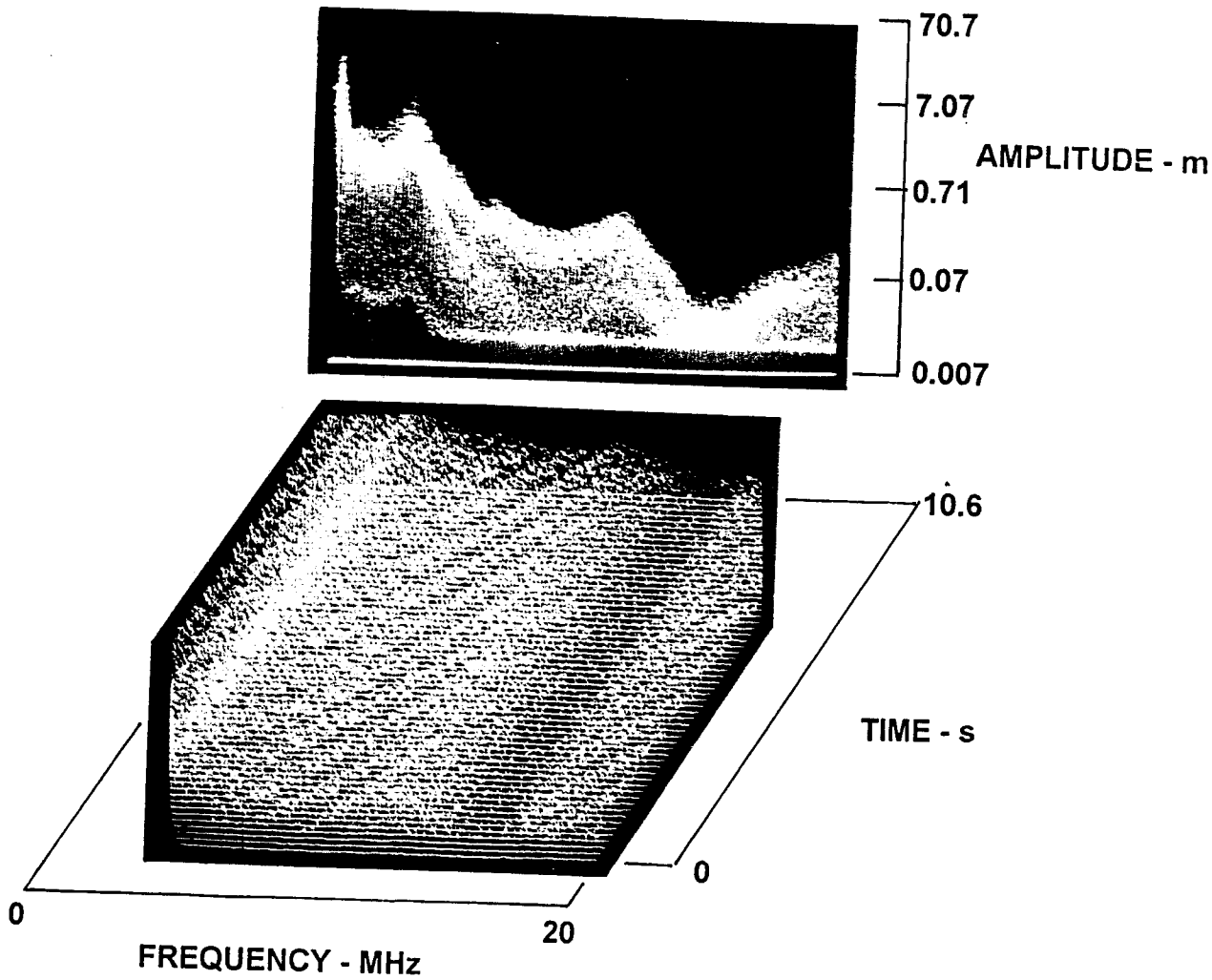

970505 1025
NW, Rm 191, 110-V Power Conduit
to Motor Controller
10 MHz, 20 MHz, 30 kHz, 100 ms
F-70, -10, -10

Figure 2.4-7

EMI Current on the 120-V, Single-Phase Power Conduit for the Motor Controller

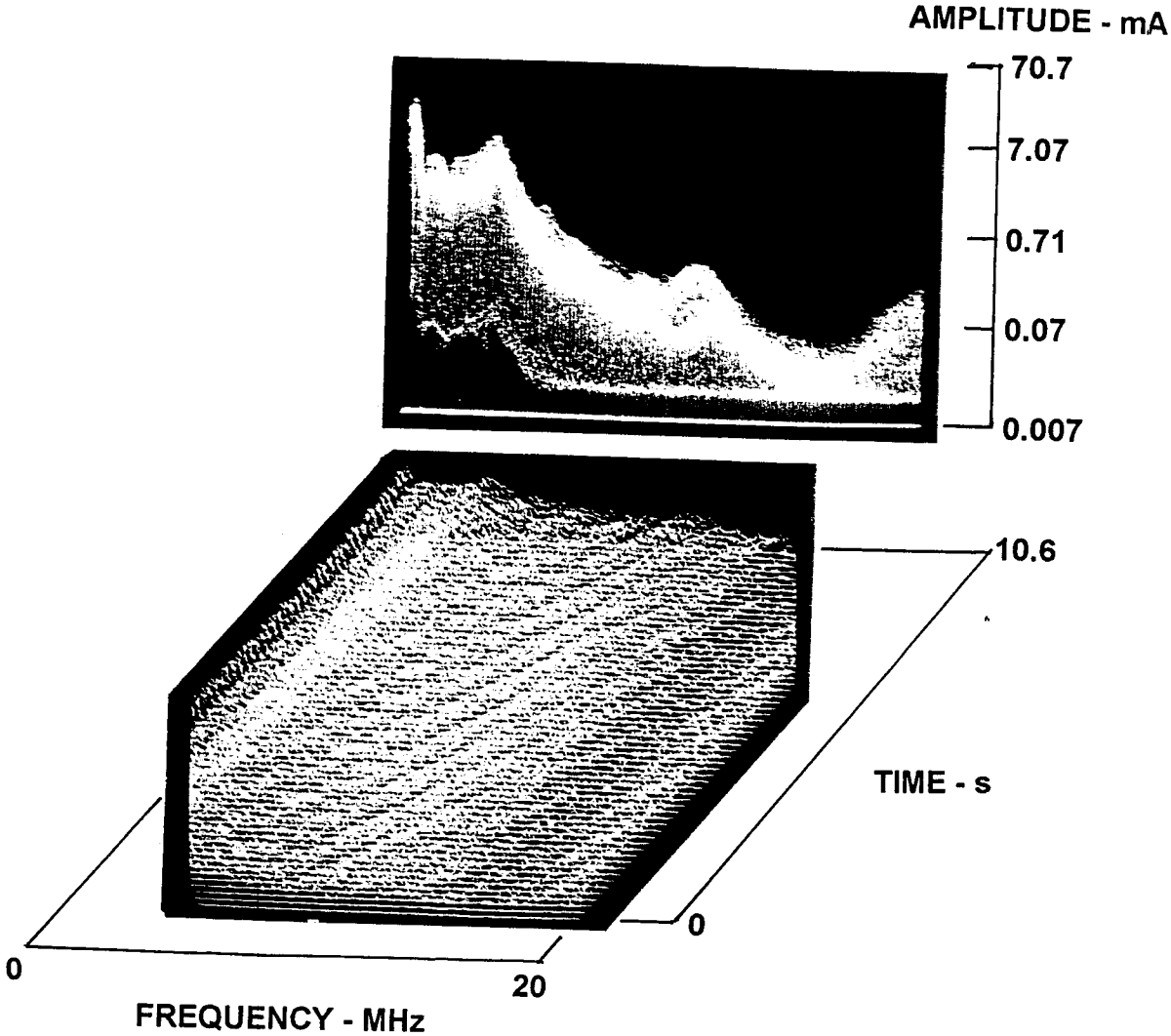

970505 1015
NW, Rm 191, Output Conduit
Motor Controller
10 MHz, 20 MHz, 30 kHz, 100 ms
F-70, -10, -10

Figure 2.4-8

EMI Current on the Conduit from the Motor Controller to the Motor

Figure 2.4-9 (970505 1245) shows the spectral and temporal properties of the EMI current flowing on the shield of the power cable running to the Coyote van. The maximum current is about 100 μA, a value high enough to produce a radiated field detectable by the site's antenna elements.

The measurements show that excessive values of EMI current from the motor-controller unit are injected onto all power conductors and onto all conduits associated with the installation. Furthermore, excessive levels of EMI current are conducted to the shield of the outside cable providing power to the Coyote van. In all likelihood, the current is also conducted to other locations throughout the building. Since the walls of the building are a mixture of concrete and brick construction, they do not provide EMI isolation. Uncontrolled penetrations through the wall allow the EMI current to flow on external cables and onto the outside walls of the Coyote van. EMI could not be detected inside the Coyote van. An inspection of the construction of the van showed that all conductors entering the van were controlled in accordance with effective integrated barrier, filter, and ground practices.

The end result is that radiation from conductors carrying excessive levels of EMI current on the Northeast side of the Operations Building produces wide-band radio fields not unlike those produced by a broad-band spread-spectrum communication system. It appears to be the collection of cables, conduits, and other conducting objects (rather than any single conductor) which radiates the harmful electromagnetic fields. This radiation is intercepted by the antenna elements on the northwest side of the building and appears as harmful radio interference at the input terminals of all receivers using Beams LBM024 and LBM036 and, to a lesser extent, receivers using other beams. <u>The motor-controller installation in Room 191, in its present configuration, is incompatible with the reception of radio signals at the site</u>.

The solution to the EMI problem is to stop the controller from injecting harmful levels of EMI current onto conductors outside its housing. This can be done by employing integrated barrier, filter, and ground techniques on the motor-controller unit. This has been done to a similar variable-speed motor-controller unit at Hanza and to other units at the Naval Postgraduate School. Since the existing motor-controller housing is unsatisfactory for the needed modifications, it will be necessary to obtain a suitable Hoffman Box and add the required filters to all conductors penetrating the box.

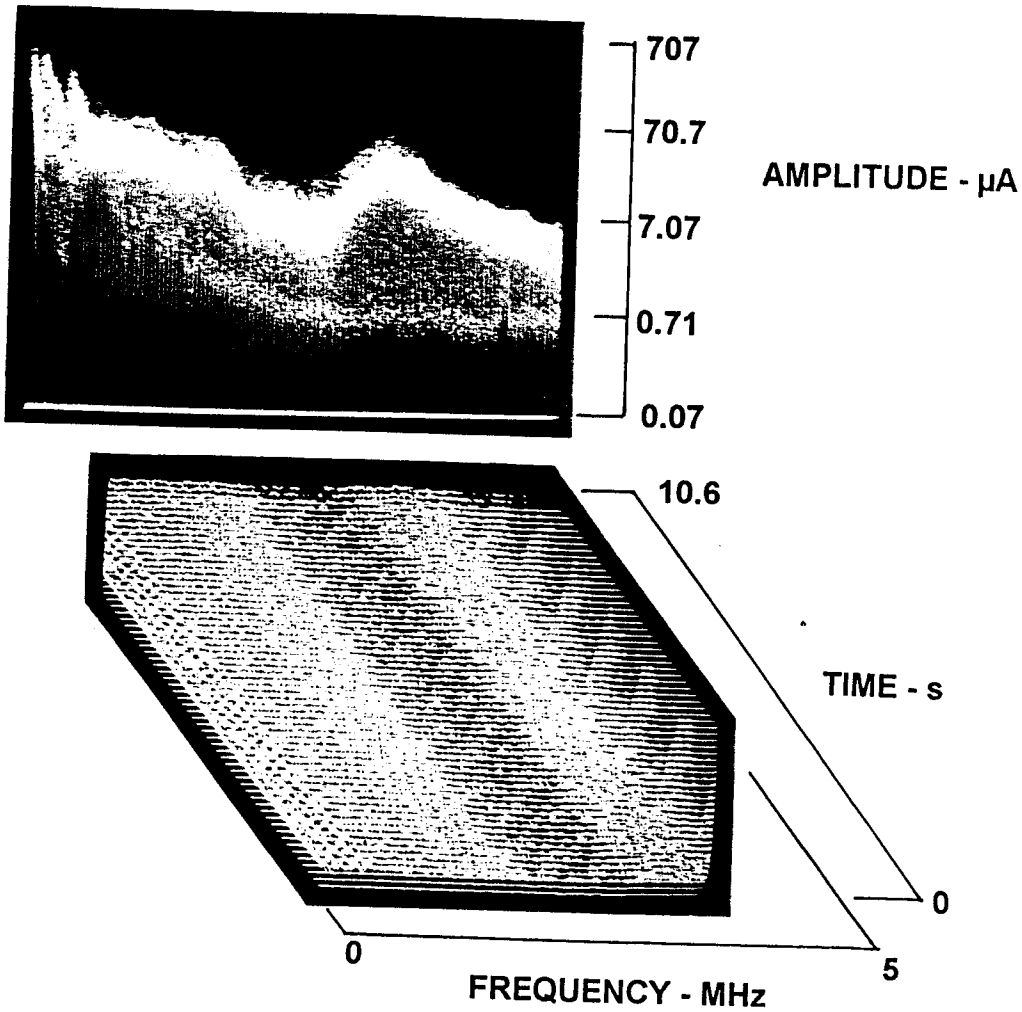

970505 1245
NW, Power Feed to Coyote Van
2.5 MHz, 5 MHz, 30 kHz, 100 ms
F-70, +20, 0, -30

Figure 2.4-9

EMI Current on the Shield of the Power Cable to the Coyote Van

2.5 UPS INTERFERENCE

Two cases of interference from Uninterruptible Power Supplies (UPS) were found at the Northwest site. One case was documented earlier as a problem by a SNEP team in 1988 (see Reference 2). It was reaffirmed as a source of harmful radio interference during the NW9705 survey. The problem unit is the site's primary UPS. Figure 2.5-1 (970429 1055) shows the temporal structure of impulsive noise from this UPS. High amplitude noise impulses are shown in the amplitude-vs.-frequency view. The straight lines in the time-history view indicate that the impulses are synchronized with the frequency of the power line. These impulses vary in amplitude as the electrical leakage paths between the UPS and the signal paths of the RFD change. These variations are caused by changes in the RF paths due to ENLARGER switching and changes in the high-frequency impedance of conducting paths of power conductors due to switching loads on and off. The UPS noise is sometimes covered up by power-line noise, but it is always present.

The NW9705 team was informed that the existing UPS was scheduled to be replaced by two new UPS units in the near future. The noise potential of the new UPS units should be determined prior to their installation. It is entirely possible that new UPS units will cause even more noise than the existing older unit; newer units tend to have faster switching times with steeper wave fronts producing higher-frequency spectral components of noise than from older units with slower switching times. The SNEP team recommends that the radio-interference potential of the new units be determined prior to purchase, and that noise-suppression techniques be implemented prior to installation.

The second case of radio interference from a UPS was traced to a SATCOM terminal operated by GE Americom. Figure 2.5-2 (970507 1528) shows impulsive noise from the UPS observed in Beam LB312. The amplitude-vs.-frequency view shows the maximum UPS noise in the region around 3.8 MHz. The noise extends upward in frequency, but at lower levels where it is covered up by other forms of man-made noise. Since the scan-time process of the instrumentation was not synchronized to the power-line frequency, the lines in the time-history view from noise impulses are slanting. An undocumented test verified that the impulses were synchronized to the power-line frequency.

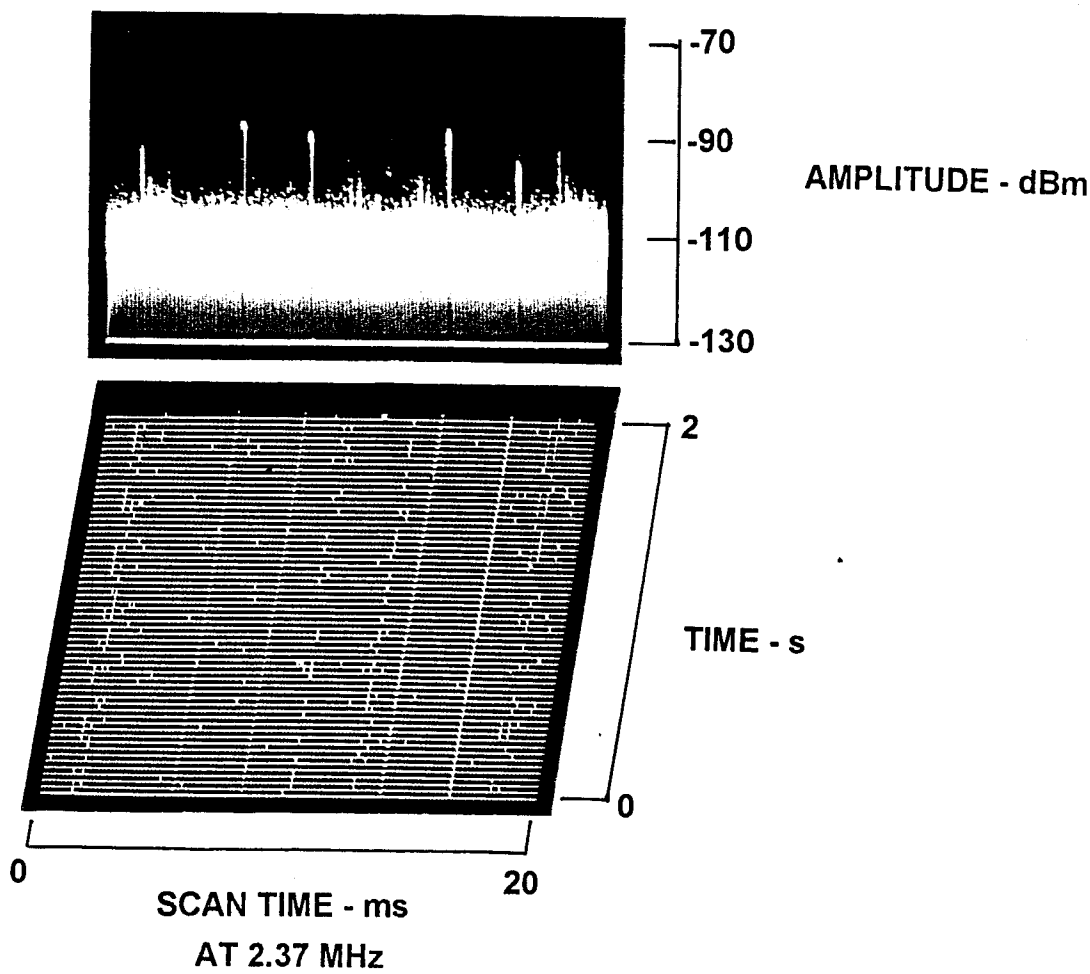

970429 1055
NW, RF Rm, LBM 060
2.37 MHz, 0, 30 kHz, 20 ms LS
BPF-1, +20, 0, -30

Figure 2.5-1

Impulsive Interference from the Site's UPS on Beam LBM 060

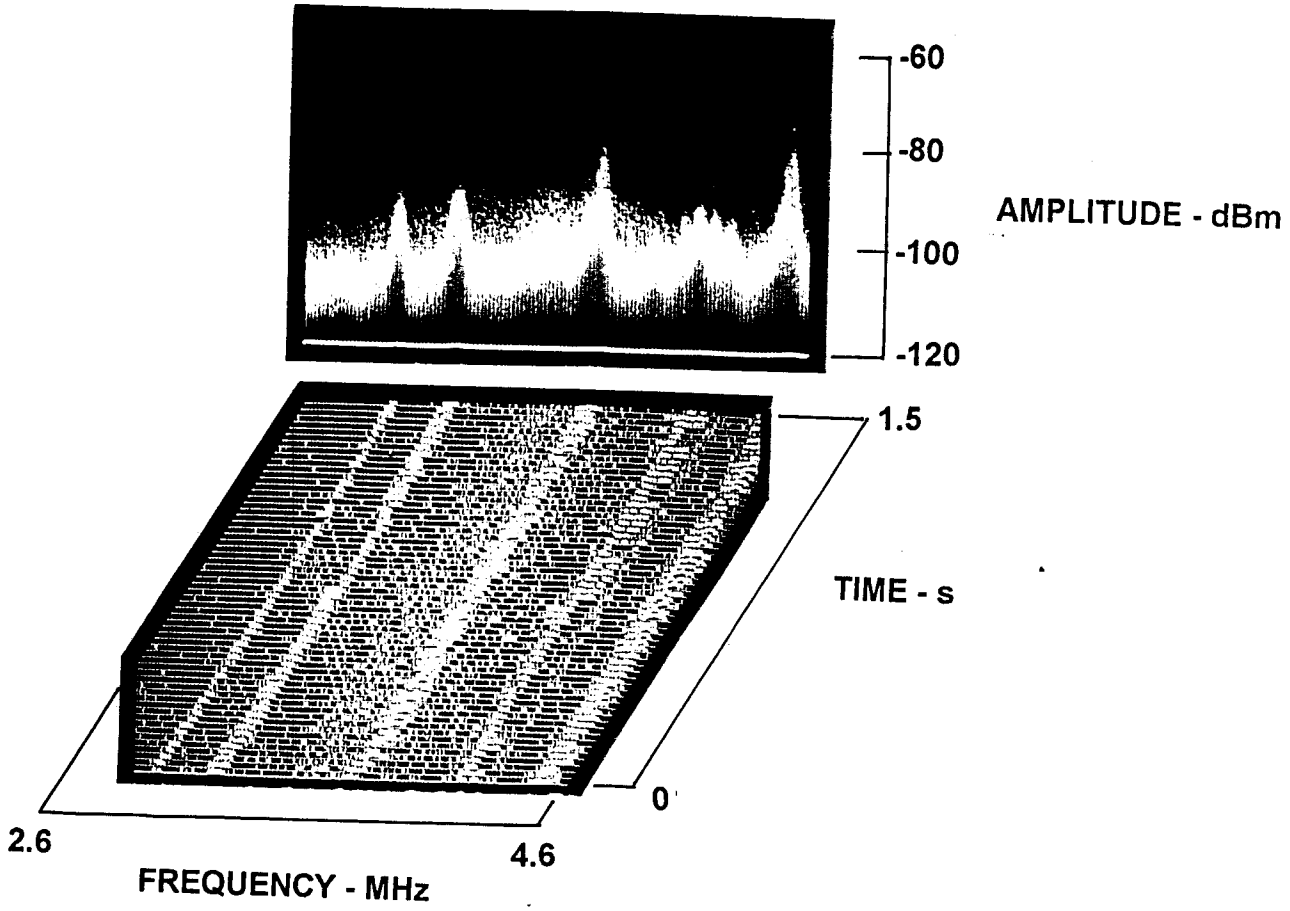

970507 1528
NW, RFD, LBM 312
3.6 MHz, 2 MHz, 30 kHz, 20 ms
BPF-1, +20, 0, -20
Noise from GE AMERICOM SATCOM
Terminal UPS - Deltec 8206A-1

Figure 2.5-2

Impulsive Interference from a UPS in the GE Americom SATCOM Shelter

The SATCOM Shelter operated by GE Americom was visited and some data was obtained at the facility. Figure 2.5-3 (970507 1450) shows the spectral and temporal structure of the UPS noise radiated from the facility over a portion of the HF band centered at 5.6 MHz. The temporal characteristics of the radiated noise are identical to those observed at the CDAA site on Beam LBM312.

The EMI current on the conduit for the input power into the UPS was examined. Figure 2.5-4 (970507 1426) shows the coarse-scale spectral and temporal structure of the impulsive noise generated by the UPS. The amplitude-vs.-frequency view shows that the spectral structure was very complex. The maximum EMI current was about 0.7 mA at a frequency near 2 MHz. The noise amplitude decreased at higher frequencies, but it remained at high levels up to about 20 MHz. Above that frequency the lower amplitude suggests it would not be a serious source of interference at the upper end of the CDAA high-band frequencies. The impulses generated by the UPS were so closely spaced that they cannot be resolved in the time-history view.

EMI current on the shield of the cable connecting the SATCOM site's TWT unit to its power supply was also examined. Figure 2.5-5 (970507 1444) shows the spectral structure of the EMI current on this cable over the frequency range from 0 to 50 MHz. The maximum EMI current is at the low end of the frequency scale, and it exceeded 7 mA. High EMI current is shown at frequencies throughout the HF band.

The data suggest that EMI current from the UPS will be found on conductors inside and outside the facility. The outside data shown in Figure 2.5-3 clearly indicates that EMI current is carried on conductors penetrating the SATCOM shelter and probably is on the outside surface of the shelter. Radiation from the outside conductors is received at the CDAA site as harmful radio interference.

Since the GE-Americom UPS is a relatively small size, about 15 kVA, the EMI problem probably can be corrected by the application of standard BFG techniques. It may be possible to keep the EMI current from escaping the UPS cabinet. It also may be possible to prevent harmful levels of EMI current from penetrating the walls of the SATCOM shelter. Both approaches need to be investigated.

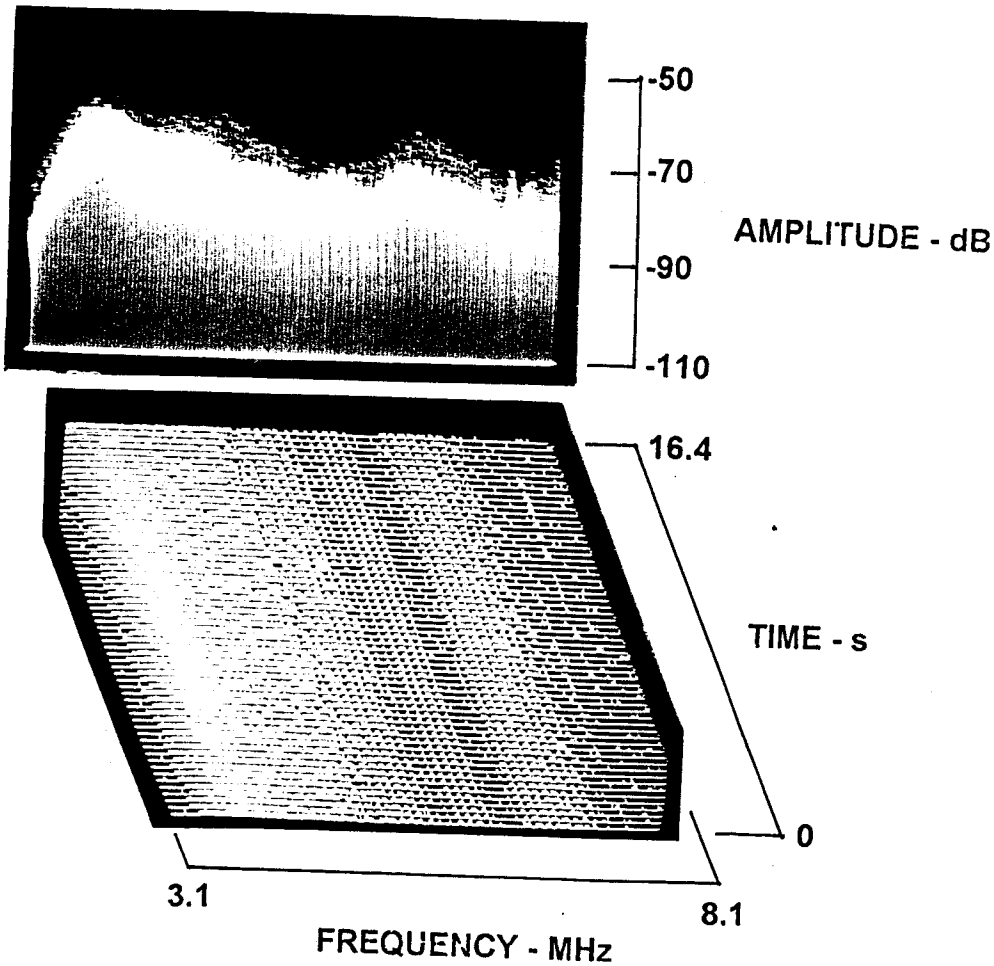

970507 1450
NW, GE AMERICOM SAT SHELTER
HF Whip 25' West of Door
5.6 MHz, 5 MHz, 30 kHz, 200 ms
0, 0, -30

Figure 2.5-3

Radiation from the GE-Americom SATCOM Shelter

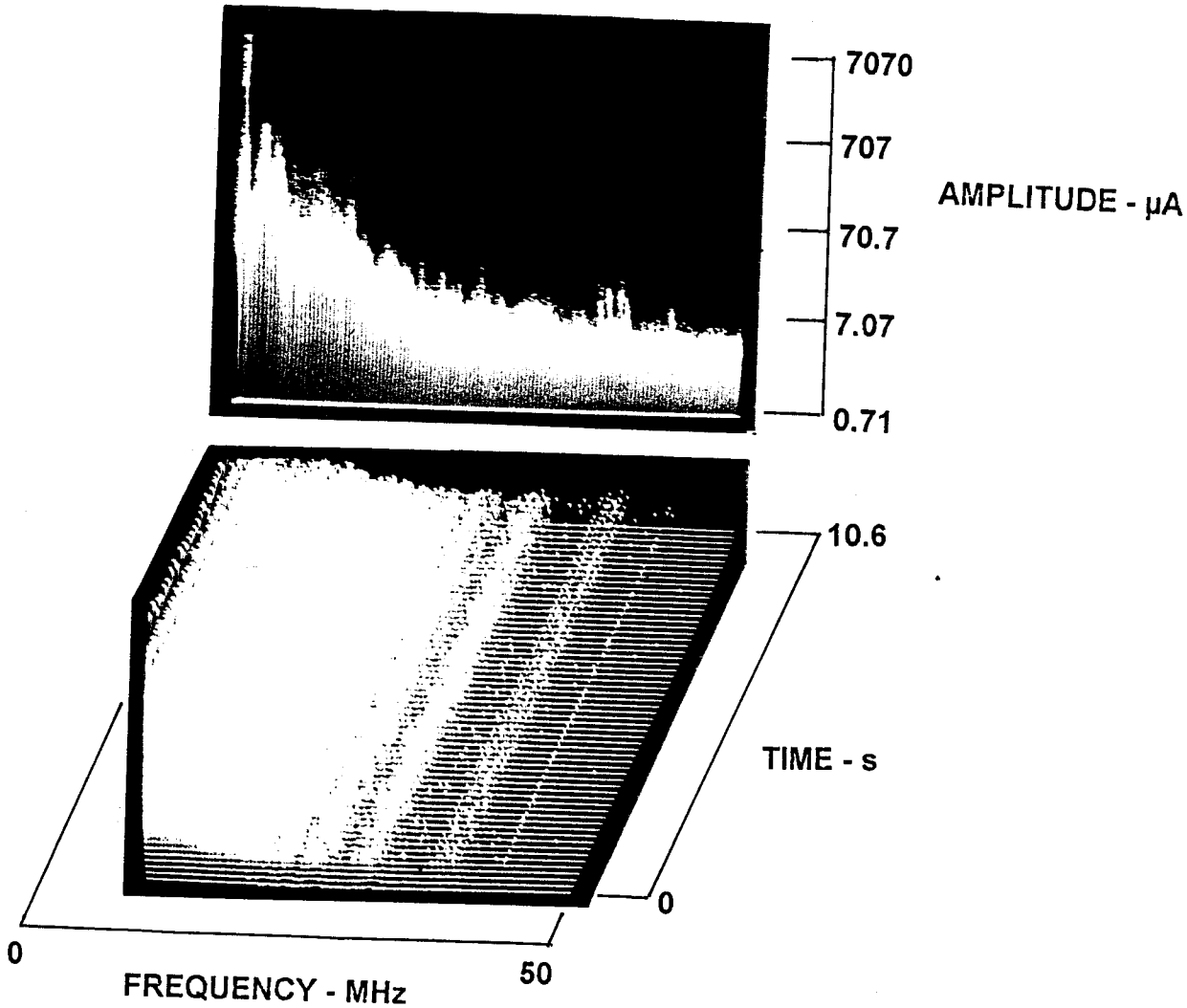

970507 1426
NW, GE AMERICOM SAT SHELTER
UPS Input Power Cable Conduit
25 MHz, 50 MHz, 30 kHz, 100 ms
F-70, 0, -30

Figure 2.5-4

EMI Current on UPS Input Power Conduit

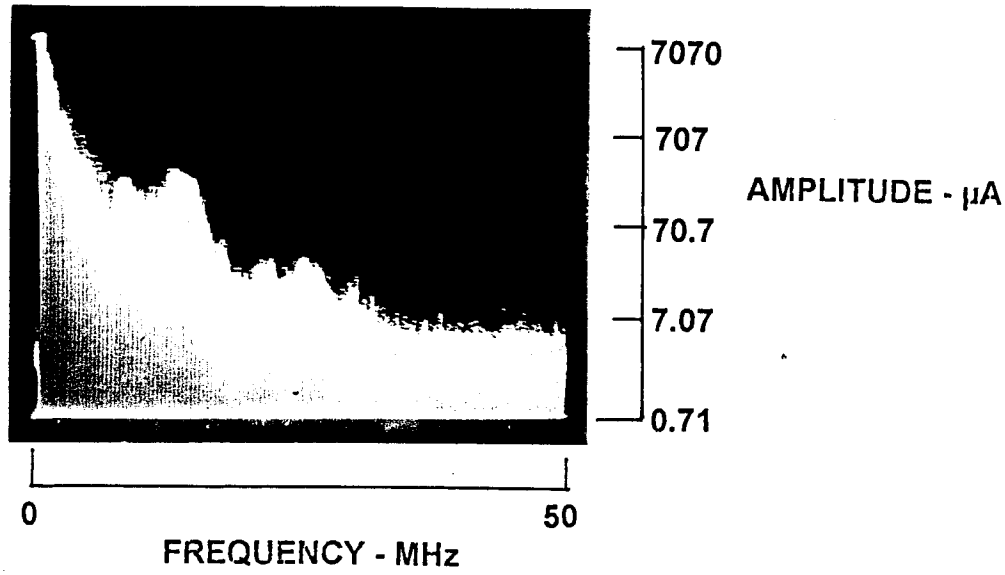

970507 1444
NW, GE AMERICOM SAT SHELTER
Pwr Cable from Pwr Supply to TWT
25 MHz, 50 MHz, 30 kHz, 200 ms
F-70, 0, -30

Figure 2.5-5

EMI Current on Shield of TWT Power Cable

The diesel generator providing emergency power to the GE Americom SATCOM facility was operated late in the survey while noise measurements were underway at the CDAA site. Radio interference from the SATCOM facility UPS increased in level when the generator was operating, and it abruptly decreased in level when the generator was turned off. Apparently, the electrical configuration of the SATCOM facility carrying EMI current changed when the generator was operated. This change resulted in a physical configuration of conductors which enhanced the radiation of broad-band electromagnetic fields associated with the flow of EMI current. In this particular instance, the reason for a temporary increase in the radio interference level at the CDAA site was identified.

The team did not have sufficient time to fully investigate the electrical properties of the cabinet housing the UPS device, the shelter, or the generator facility. This is the first step in defining a successful mitigation process. Space must be available for the installation of filters on all penetrating conductors of the UPS cabinet or the shelter provided the UPS cabinet and/or the shelter can provide suitable electromagnetic shielding. It will be necessary to more completely examine the shelter and the UPS before a final recommendation can be made regarding the best method to mitigate the SATCOM UPS radio-interference problem. The cooperation of the site managers must be obtained prior to modifying their facilities.

2.6 NATO SATCOM GENERATOR INTERFERENCE

During the investigation of sources of interference from the variable-speed motor drive in Room 191 and the UPS in the SATCOM facility operated by GE Amercom, a third source of interference was located. A digital device had recently been installed to control the field current in two diesel generators at the NATO SATCOM facility located northeast from the CDAA. A general search of the building with a Radar Engineers Model 245 EMI Sniffer showed that all electrical and other metal conductors associated with the motor-generator units carried EMI current as well as building structural elements in the near vicinity of the generator room.

Since the Model 245 Circuit Sniffer does not provide calibrated values of EMI current, additional instrumentation was moved to the NATO SATCOM facility. Figure 2.6-1 (970507 1045) shows EMI current flowing on one of the two motor-generator field-excitation cables over the range from 0 to 100 MHz. The upper amplitude-vs.-frequency view shows the amplitude of the current; the maximum current was about 0.5 mA at a frequency near 5 MHz. The current gradually decreases in amplitude with increasing frequency, but it is still more than 10 μA in amplitude at 100 MHz. The spectral shape contains numerous minor nulls and peaks. The time-history view shows that the EMI current is continuous with time and does not change in spectral or temporal content during normal standby operation of the generator.

Figure 2.6-2 (970507 1047) shows the fine-scale temporal structure of the EMI current flowing on the conduit housing the conductors carrying the field excitation current. The data was obtained at a frequency of 50 MHz. The temporal structure provides a distinctive signature useful for recognition of the interference.

Additional measurements were made to examine the flow of EMI current on other parts of the generator unit. Figure 2.6-3 (970507 1032) shows EMI current on the shield of the output conductors of the generator over the frequency range of 0 to 100 MHz. The spectral and temporal properties of the EMI current are similar to those shown in Figure 2.6-1 for the field excitation cable. A single discrete-frequency spectral component is shown at about 90 MHz. This is current induced in the shield by a local FM station.

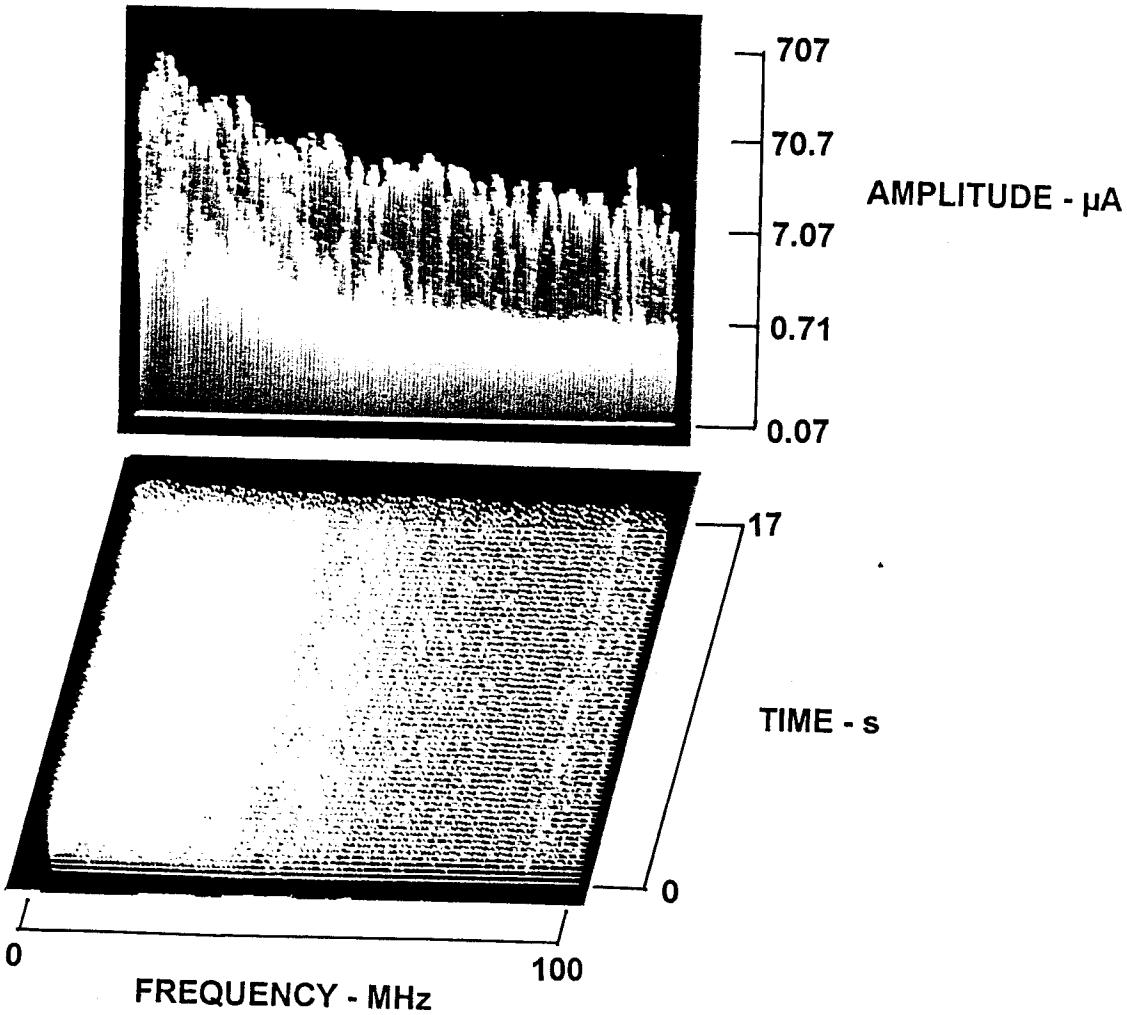

970507 1045
NW, NATO SATCOM
MG Field Excitation Cable
50 MHz, 100 MHz, 30 kHz, 200 ms LS
F-70, +20, 0, -30
F-70 clamped on cable in raceway

Figure 2.6-1

EMI Current of the Field Excitation Cable

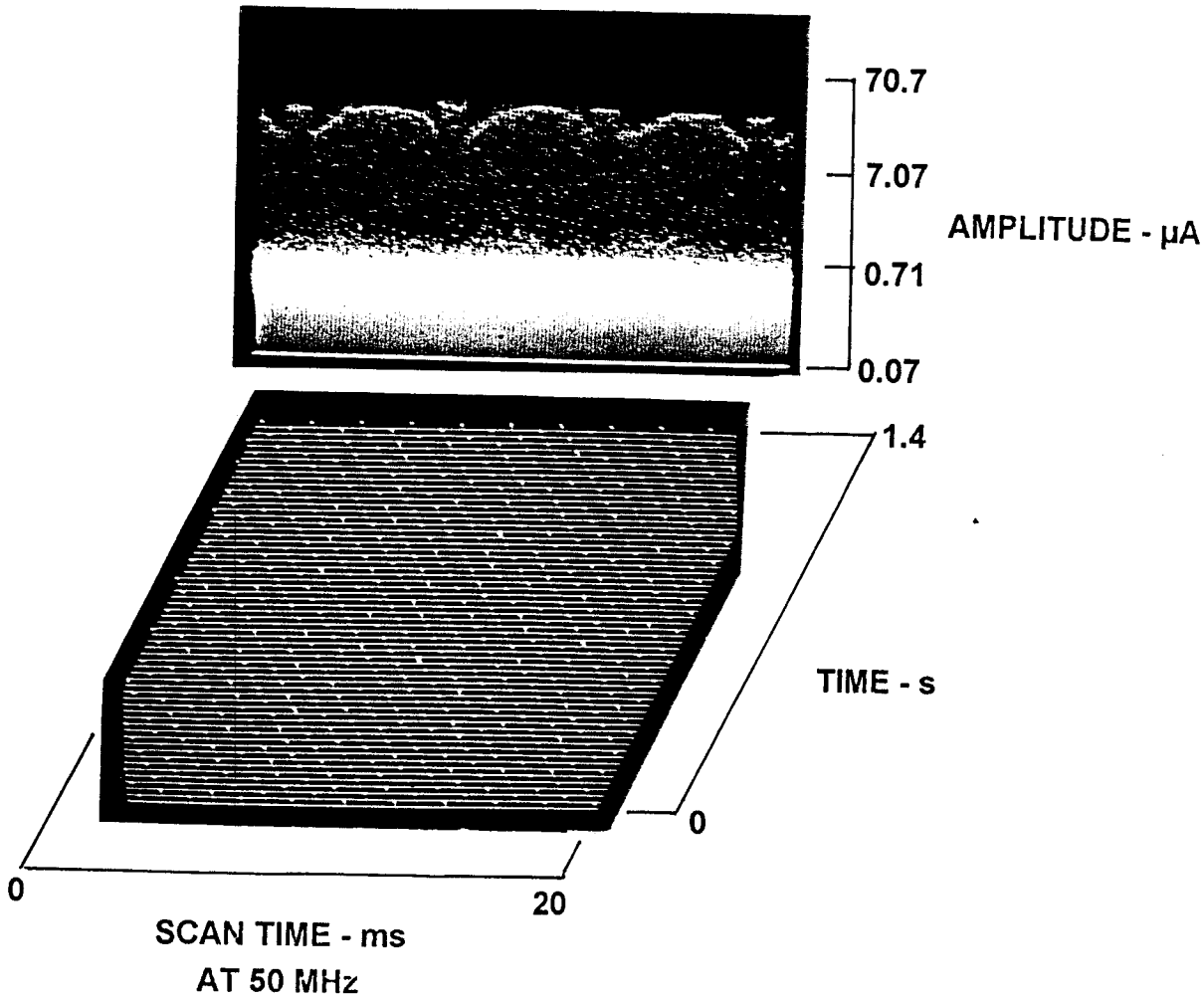

970507 1047
NW, NATO SATCOM, Gen Rm
Field Excitation Conduit
50 MHz, 0, 30 kHz, 20 ms
F-70, +20, 0, -30

Figure 2.6-2

Fine-Scale Temporal Structure of EMI Current on the Field Excitation Cable

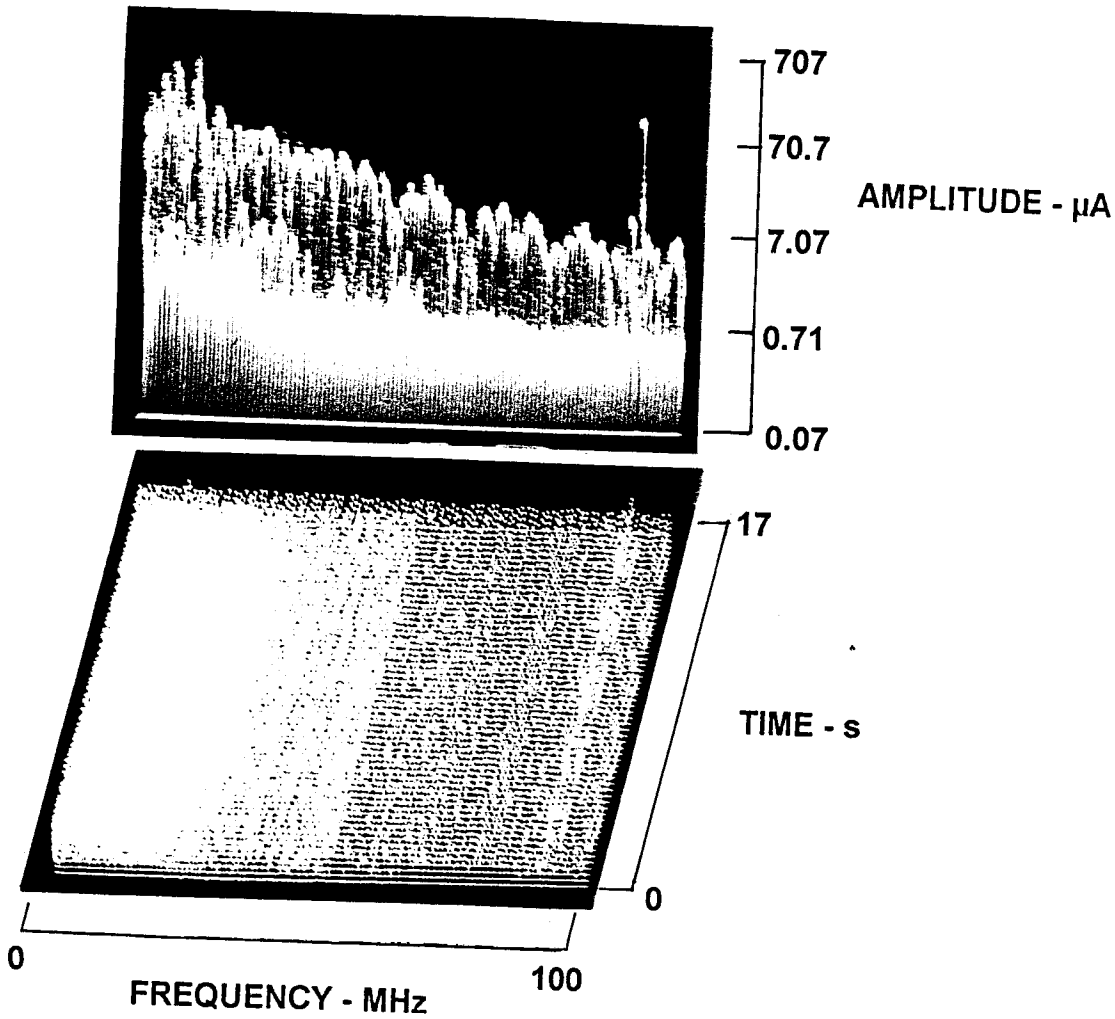

970507 1032
NW, NATO SATCOM
MG Output Cable
50 MHz, 100 MHz, 30 kHz, 200 ms LS
F-70, +20, 0, -30

Figure 2.6-3

EMI Current on the Generator Output Conductors

Figure 2.6-4 (970507 1030) shows EMI current flowing on the generator ground cable over the frequency range from 0 to 100 MHz. The maximum EMI current was about 200 μA over a broad band of frequencies below 10 MHz. It decreased as frequency increased. While the current on the ground conductor is less than the current flowing on the electrical conductors, it indicates that substantial amounts of HF and VHF EMI current are flowing on the physical structure of the generator as well as on its associated electrical wires.

Figure 2.6-5 (970507 1019) provides another example of EMI current flowing on a physical part of the generator, the oil pump control line. The frequency range of the data is from 0 to 100 MHz and the spectral shape is roughly similar to that of the current flowing on the ground conductor. Two discrete-frequency spectral components are shown near 90 MHz. Both are signals from local FM stations. The metal configuration of the generator acts as an antenna and intercepts radio fields from the FM stations which then produce current on the structure.

The Radar Engineers Model 245 Circuit Sniffer indicates that high levels of EMI current are flowing on other mechanical components in the generator room and on conducting material in its structure. The physical configuration of the F-70 probe is not suitable for the measurement of current on these conductors and the SNEP team did not anticipate the need for special probes for such measurements. Nevertheless, the data obtained is sufficient to show that EMI current is conducted from its source onto many other nearby conductors. It is a general site problem rather than a problem confined to electrical conductors associated with the generator field coils.

Discussions with the operators of the NATO SATCOM facility indicate that the emergency power system was recently installed and had not yet been accepted from the installation contractor. Manuals for the field-control unit have not been provided, thus the operators had little information about its details or its operation. In addition, since all modifications to a NATO facility must be approved by a governing body located elsewhere, it is not clear how to proceed with the mitigation of the EMI. This problem will require additional coordination between NSGA Northwest and the operators of the NATO SATCOM facility.

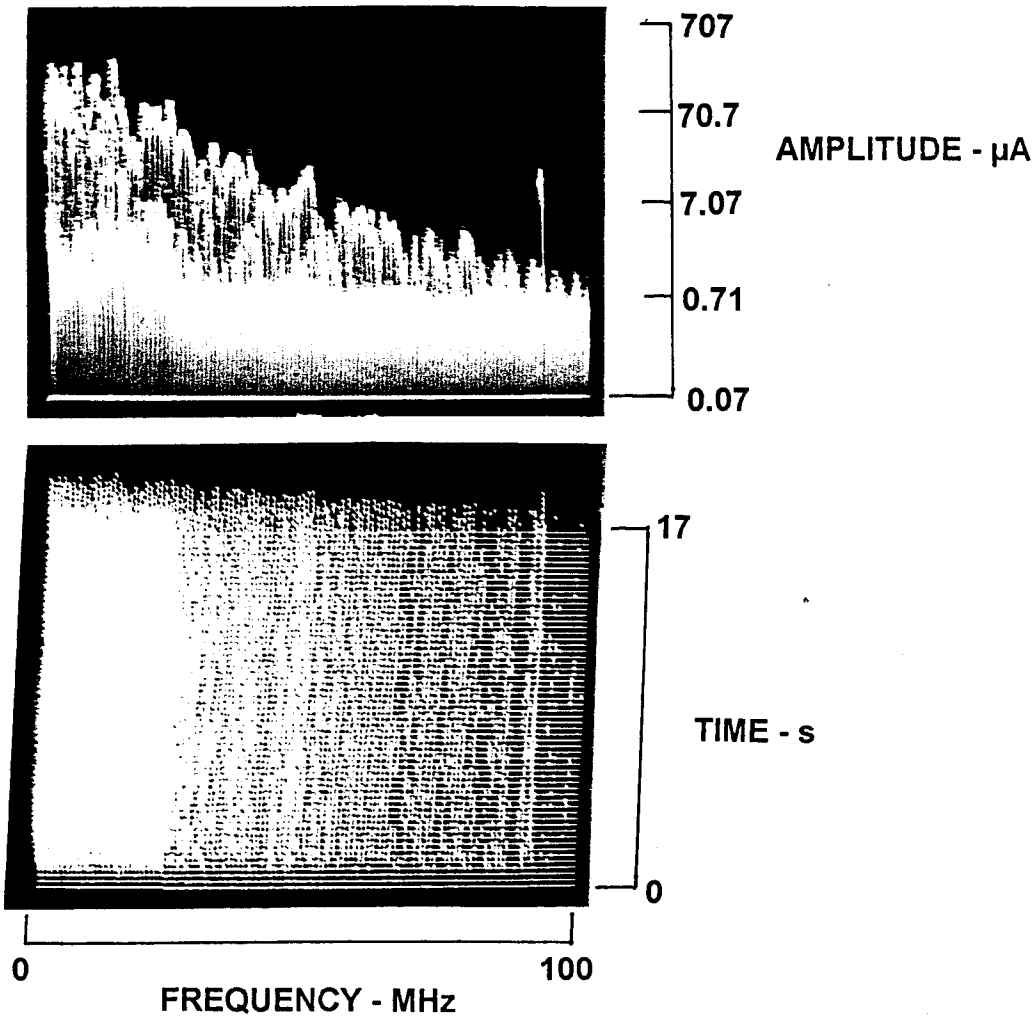

970507 1030
NW, NATO SATCOM
MG Chassis Gnd Wire
50 MHz, 100 MHz, 30 kHz, 200 ms LS
F-70, +20, 0, -30

Figure 2.6-4

EMI Current on Generator Ground Wire

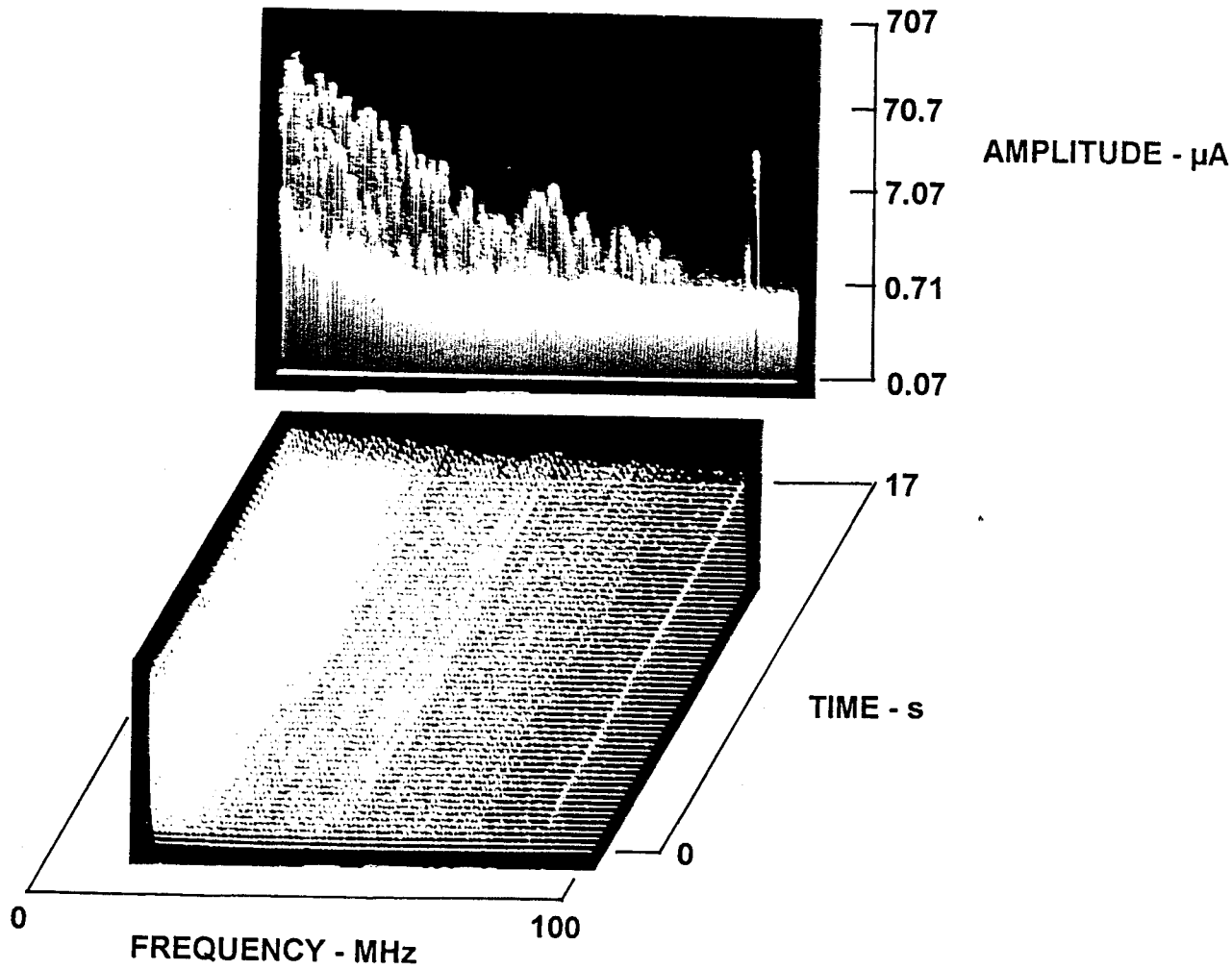

970507 1019
NW, NATO SATCOM
Oil Pump Control Line for MG
50 MHz, 100 MHz, 30 kHz, 200 ms LS
F-70, +20, 0, -30

Figure 2.6-5

EMI Current on Generator Oil Pump Line

2.7 FLUORESCENT LIGHTS

Radio interference from fluorescent lights has been of concern for a number of years. While examples of severe noise from a faulty ballast and faulty lights have been noted, these kinds of problems can be corrected by maintenance actions. It is the impact of the continuous, low-level interference produced by ballasts and fixtures that was of concern. In addition, some of the new electronic-ballast lights had been installed at the Northwest site.

Preliminary tests on both the magnetic- and electronic-ballast types of lights indicate that they produce high enough levels of radio interference to be of concern when used in HF and VHF receiving sites.[4] Because of this concern, some time was used in an attempt to better understand the interference potential at Northwest of fluorescent lights equipped with standard magnetic ballast and with the new electronic ballast. Lights with a standard magnetic ballast were used in the RF Room. Lights with electronic ballasts were used in a large hallway outside the RF room. The availability of both types of lights in the site provided a convenient test bed.

The first step was to measure the EMI current on conduits feeding the lights and on light fixture support wires. Figure 2.7-1 (970501 1530) shows EMI current on the conduit feeding a bank of fluorescent lights with magnetic ballasts. The figure shows the EMI current level over the frequency range from 100 kHz to 2 MHz. Data below 100 kHz is uncalibrated because the response of the F-70 probe falls rapidly below that frequency. Measurements at higher frequencies indicate that the EMI current levels on the conduit are very low and of no concern. The upper view of amplitude-vs.-frequency shows a complex spectral shape containing multiple components. The temporal data show that the current consists of close-spaced impulses synchronized with the power-line frequency. The maximum current was about 200 μA at a frequency near 500 kHz.

EMI current on the conductors was not measured since the conductors were inside the conduit and not accessible. There was not time to disassemble the conduit and obtain access to the conductors. Since most of the harmful EMI radiation was believed to be from the conduit rather than from the enclosed conductors, little emphasis was given to the need for direct measurements on the conductors.

---

[4] Robert M Perry, Wilbur R. Vincent, Richard W. Adler, and Scott S. Shillcock, *Radio Interference from Fluorescent Lights Using Energy Efficient Electronic Ballasts*, Technical Report NPS-EC-011, Naval Postgraduate School, Monterey, CA, November 1995.

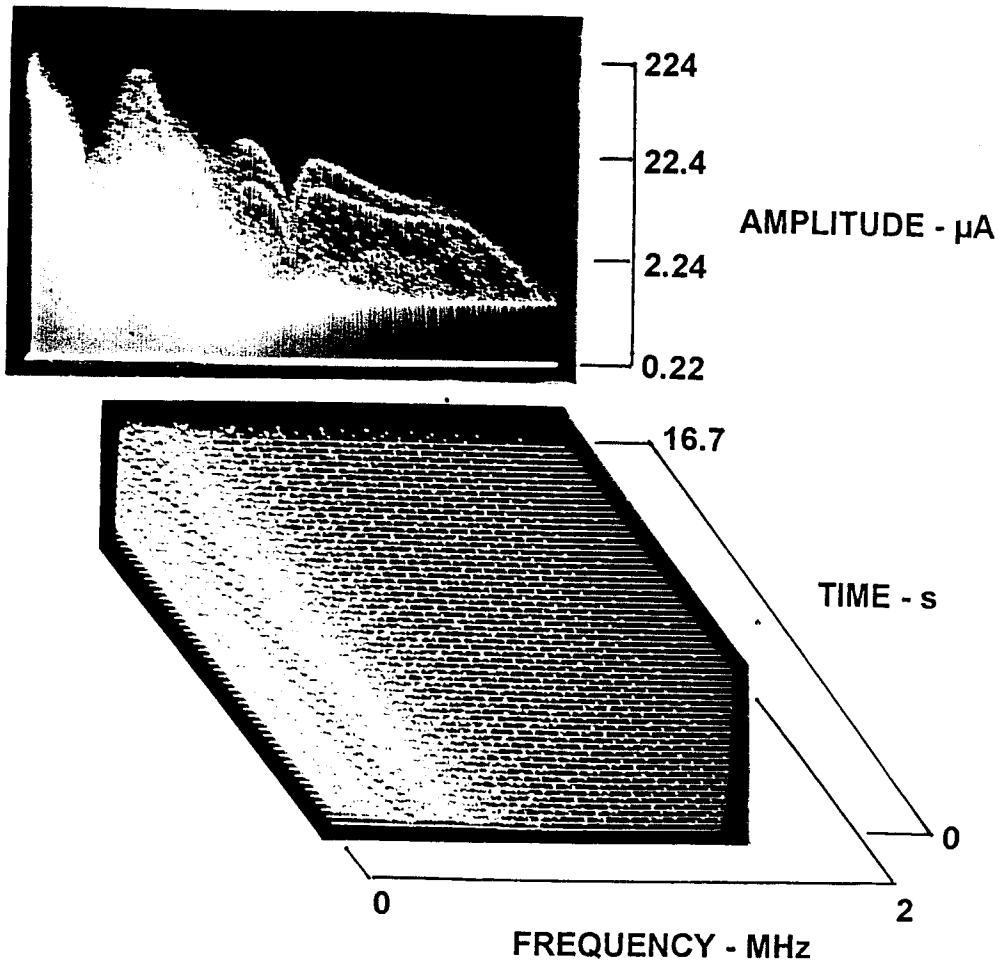

970501 1530
NW, RFD, Metal conduit feeding bank
of fluorescent lights, MB
1 MHz, 2 MHz, 30 kHz, 200 ms
F-70, +20, 0, -20

Figure 2.7-1

EMI Current on Conduit Feeding Fluorescent Lights with Magnetic Ballast

Figure 2.7-2 (970501 1513) shows that some of the EMI current was conducted along the light fixture support wires. These wires were attached to metal structural parts of the ceiling immediately above the light fixtures. This data indicates that EMI current flowing in the building structural material must be considered as well as EMI current on the conductors and conduits providing power to the lights.

Additional measurements of the EMI current on conduits providing power to the fluorescent lights raised questions about the magnitude of that portion of the EMI current on the conduit generated by the fluorescent lights. Figure 2.7-3 (970501 1427) shows that the EMI current changes significantly with time while the lights remain on and undisturbed. The time-variations of the EMI current are shown in the time-history view. Figure 2.7-4 (970501 1420) is another view of the same observation. A burst of EMI current that cannot be attributed to the lights occurred during the measurement. Apparently, the primary source of the EMI current on the conduits feeding the lights was from sources elsewhere in the Operations Building.

Figure 2.7-5 (970502 1355) provides another case where a burst of current from a switching transient appeared on the conduit feeding a fluorescent light. That portion of the data containing the transient was expanded to obtain a better view of the spectral structure of the transient. It is shown in the amplitude-vs.-frequency view.

Figures 2.7-3 through 2.7-5 provide direct evidence that the EMI current observed on conductors associated with the fluorescent lights was primarily from other sources in the Operations Building. While some portion of this current may have been generated by the lights, there was not sufficient time to separate noise from the two sources. The primary high-frequency components shown are from other sources.

This data does not answer the question of radio noise from the lights. It merely says that other sources are more significant. Radio noise from fluorescent lights might be a concern in a noise-quiet site, but it is not the most severe problem at Northwest at this time.

Current on the conduit feeding a light fixture at the fundamental and low-order harmonics was also examined. Figure 2.7-6 (970502 1108) provides amplitudes of current from 60 Hz up to the 33rd harmonic. The fundamental current is more than 8 mA while the 3rd and 5th harmonics are about 3 mA.. These seem unusually high, and they would produce unusually high transients should incidental contact be made between the conduit and another metal object.